

# Geometrical aspects of Gigantic Magneto-Electric effect and Quantum Pump

Ryuichi Shindou<sup>1</sup> and Naoto Nagaosa<sup>1,2</sup>

<sup>1</sup>*Department of Applied Physics, University of Tokyo, Bunkyo-ku, Tokyo 113-8656, Japan*

<sup>2</sup>*CERC, AIST Tsukuba Central 4, Tsukuba 305-8562, Japan*

(Dated: December 18, 2019)

We study the Magneto-Electric (ME) effect from the viewpoint of the Berry phase connection and quantum adiabatic charge transport (QAPT). The linear response theory for the electronic polarization  $\vec{P}_{\text{el}}$  can be interpreted in terms of the flux or the fictitious magnetic field related to the Berry phase in the generalized space which is composed of crystal momentum and some external parameters. An applied magnetic field modifies the spin configuration, which induces adiabatic deformation of the Bloch wavefunction and results in the electronic polarization given by the total flux penetrating the plaquette spanned by this external parameter and crystal momentum. This provides a new mechanism for the gigantic ME effect. For a cyclic change of the applied magnetic field, even a quantized charge transport is possible.

PACS numbers: 72.20.My, 75.45.+j, 75.80.+q

## I. INTRODUCTION

The interplay between the spin and charge degrees of freedom is one of the central issues in the physics of strongly correlated electronic systems. From this viewpoint, the cross correlation between these two degrees of freedom is of particular interests. The Magneto-Electric (ME) effect is a phenomenon where the magnetization  $\vec{M}$  appears under the applied electric field  $\vec{E}$  or the electric polarization  $\vec{P}$  is induced by the magnetic field  $\vec{H}$ .

This effect has been studied for a long term since its theoretical prediction<sup>1</sup> and experimental observations<sup>2</sup> in  $\text{Cr}_2\text{O}_3$ . A phenomenological description of this effect is given by the free energy containing  $\alpha_{ij}E_iH_j$ . The selection rule for the ME coefficient  $\alpha_{ij}$  is obtained from the group theoretical considerations. In case of antiferromagnetically ordered  $\text{Cr}_2\text{O}_3$ , the time-reversal symmetry ( $R$ ) accompanied by the spatial translation ( $T$ ) is broken due its peculiar crystal structure, in contrast to usual antiferromagnets. Instead, its AF ordered phase is invariant under the product of the time-reversal symmetry ( $R$ ) and the spatial inversion ( $I$ ), which does not prohibit the finite matrix element  $\alpha_{ij}$ . Furthermore, due to the several other symmetries in antiferromagnetically ordered  $\text{Cr}_2\text{O}_3$ , there remain only the diagonal matrix elements  $\alpha_{xx} = \alpha_{yy} = \alpha_{\perp}, \alpha_{zz} = \alpha_{\parallel}$ <sup>1</sup>. Microscopic theories of the ME effect in  $\text{Cr}_2\text{O}_3$  based on these phenomenological observations have been proposed<sup>3,4,5</sup>. According to these theories, an applied electric field shifts the oxygen ions  $\text{O}^{2-}$  and breaks the crystallographic equivalence between several sublattices composed of Cr atoms. For example, the g-factors on two Cr sublattices differ from each other due to the crystal field produced by the shifted oxygen ions. This difference induces a finite net magnetization<sup>3</sup>. A temperature dependence of  $\alpha_{\parallel}$  seems to be well explained by this mechanism<sup>3,5</sup>. When we trace these theories the other way around, a microscopic origin for the *electric polarization* induced by an applied magnetic field was attributed to the displacement of the ligand anion

atoms, namely the lattice displacements.

Instead, we are going to study a *Bloch electron's contribution* to the macroscopic electronic polarization (MEP) induced by the applied magnetic field. The MEP in dielectrics has been formulated only recently, since an electron's position operator is ill-defined in the Hilbert space spanned by the Bloch wavefunctions which obey the periodic Born-von Karman (BvK) boundary condition<sup>7,8</sup>. In 1990s, it is naturally recognized that the MEP induced by the lattice distortions is the averaged value of total charges which are transferred through the unit area in the system when the lattice deformations occur<sup>8</sup>. Because the lattice distortions are generally induced by the external pressure, these phenomena are nothing but the piezo-electric effects<sup>9,10</sup>.

The MEP is closely related to the quantized adiabatic particle transport which was proposed by D.J.Thouless and Q.Niu in the 1980s<sup>11</sup>. They considered the 1D band insulator with periodic boundary condition. When some external parameters are deformed adiabatically, and are put back to their initial values, the particle current integrated over this period becomes quantized to be integer times its particle unit. This integrated electron current is nothing but the total electrons flowing through the unit area during one period. Thus non-zero quantization of the integrated current means that the MEP increases by a finite amount even though the external parameters get back to their initial values. Recently these kind of the “d.c.” responses induced by the “a.c.” impulses are studied also in the context of the spin current and is generally called Quantum Pump<sup>12</sup>.

Berry phase is the quantal phase associated with the adiabatic time-evolution of the wavefunction. Let the external parameter evolve from  $\vec{\lambda}_i$  to  $\vec{\lambda}$  along the path  $\Gamma$ <sup>13</sup>, the adiabatically evolved wavefunction  $|\Psi(\vec{\lambda}(t), t)\rangle$  is given as follows.

$$|\Psi(\vec{\lambda}, t)\rangle = e^{-\int_{\Gamma}^{\vec{\lambda}_i \rightarrow \vec{\lambda}} \langle \Psi_{\text{inst}}(\vec{\lambda}') | \vec{\nabla}_{\vec{\lambda}'} | \Psi_{\text{inst}}(\vec{\lambda}') \rangle \cdot d\vec{\lambda}'} |\Psi_{\text{inst}}(\vec{\lambda})\rangle, \quad (1)$$

where  $|\Psi_{\text{inst}}(\vec{\lambda})\rangle$  is the instantaneous eigenstate of the corresponding time-dependent Hamiltonian  $\hat{H}(\vec{\lambda}(t))$ , and we take the initial wavefunction  $|\Psi(\vec{\lambda}(t_i) \equiv \vec{\lambda}_i, t_i)\rangle$  as  $|\Psi_{\text{inst}}(\vec{\lambda}_i)\rangle$ . The r.h.s. of eq.(1) is invariant under the U(1) gauge transformation;  $|\Psi_{\text{inst}}(\vec{\lambda})\rangle \rightarrow e^{i\theta(\vec{\lambda})}|\tilde{\Psi}_{\text{inst}}(\vec{\lambda})\rangle$  where  $\theta(\vec{\lambda}_i) = 0$ . When we take  $\vec{\lambda}(t = t_f) \equiv \vec{\lambda}_f$  to the initial parameter, i.e.,  $\vec{\lambda}_f = \vec{\lambda}_i$ , total phase factor the w.f. acquires, which is called U(1) phase holonomy, can be given by the surface-integral of the *flux* over the arbitrary surface  $S$  whose boundary is the loop  $\Gamma_{\text{cyc}}$ ;

$$e^{-\oint_{\Gamma_{\text{cyc}}} \langle \Psi_{\text{inst}}(\vec{\lambda}) | \vec{\nabla}_{\vec{\lambda}} | \Psi_{\text{inst}}(\vec{\lambda}) \rangle \cdot d\vec{\lambda}} = e^{-i \int_S \vec{B}(\vec{\lambda}) \cdot d\vec{S}}$$

where the flux is defined as follows;

$$\vec{B}(\vec{\lambda}) \equiv -i \vec{\nabla}_{\vec{\lambda}} \times \langle \Psi_{\text{inst}}(\vec{\lambda}) | \vec{\nabla}_{\vec{\lambda}} | \Psi_{\text{inst}}(\vec{\lambda}) \rangle. \quad (2)$$

Since this flux is independent of the gauge choice of the instantaneous eigenstate,  $\vec{B}(\vec{\lambda})$  is also called *fictitious magnetic field*, while  $\vec{A}(\vec{\lambda}) \equiv \langle \Psi_{\text{inst}}(\vec{\lambda}) | \vec{\nabla}_{\vec{\lambda}} | \Psi_{\text{inst}}(\vec{\lambda}) \rangle$  corresponds to its associated vector potential. This kind of the flux also appears in the context of the MEP and/or the Quantum Pump, since the current is represented by the derivative of the phase of the wavefunctions. Therefore the integrated particle current can be viewed as the flux penetrating the plaquette spanned by the crystal momentum and the deformed external parameter. Although the definitions of the flux are slightly modified from that of eq.(2) (see eqs.(8,9)), both of these flux are essentially same mathematical objects, which are called field strengths associated with the U(1) Fiber bundle. And the point where the energy degeneracy occurs plays a role of the source of these flux, so to speak, fictitious magnetic charge. Generally speaking, this source of the flux, which is called Dirac monopole, is an origin of the nontrivial structure of the U(1) Fiber bundle associated with U(1) phase factors of the wavefunctions<sup>14</sup>.

Recently the spontaneous (anomalous) Hall current observed in some magnets is discussed in the context of the integer quantum Hall current, where the story shares the common concepts with the MEP and/or the Berry phase holonomy associated with the adiabatic evolutions<sup>15</sup>. Namely, the Hall conductivity, for example  $\sigma_{xy}$ , is given by the total flux penetrating the plaquette (2D magnetic Brillouin zone) spanned by  $x$ -component of the crystal momentum and its  $y$ -component<sup>16</sup>. There it turned out that the non-coplanar spin configuration and/or the spin-orbit coupling generate the Dirac monopoles and thus the nontrivial distribution of the flux in the crystal momentum space which results in the anomalous Hall effect.

In this paper we study the MEP induced by the deformation of the background spin configurations in the magnetic materials. Since the spin ordering fields (external parameters) in the magnetic systems can be controlled by the applied magnetic field, this corresponds to the electronic contribution to the ME effect. The focus of this paper is the ME effect due to this Berry phase connection and the nontrivial distribution of the flux associated

with the magnetic Bloch wavefunctions in magnetic materials. In this sense the MEP and the transverse conductivity  $\sigma_{xy}$  are closely related, namely these two physical quantities are the different component of the same field in the generalized momentum space. Therefore the quantized charge transport for a cyclic change  $\Gamma_{\text{cyc}}$  is possible through the analogy of the integer quantum Hall effect, i.e., both of them are related to the first Chern numbers associated with the filled bands. In general, a non-zero quantization of the total charge transport induced by the adiabatic change of some external parameters requires the broken spatial inversion symmetry, while that of the Hall conductivity requires the broken time reversal symmetry.

The main results obtained in this paper are summarized as follows. From the viewpoint of the perturbation theory, the ME effect was known to be enhanced when the energy denominator is small, i.e., when the band gap is small. However we propose, in this paper, a new mechanism of the magnetoelectric effect, where it is revealed that not only the band gap reduction but also the U(1) phase associated with the magnetic Bloch wavefunction play very important roles in determining the magnitude of the ME effect. We classify the magnetic dielectrics into two categories from this viewpoints. One has the nontrivial structure of the U(1) Fiber bundle associated with the magnetic Bloch wavefunction, while the other does not. Former categories are the good candidates to which our mechanism can be applied. There the nontrivial topological structure is originated from the band crossing located in the parameter space. Secondly we construct two models where such a non-trivial structure of the Fiber bundle are realized and the gigantic electronic polarizations are induced by the applied magnetic field. Their magnitudes amount to the order of  $\frac{e}{a^2} \sim 1$  [C/m<sup>2</sup>], where  $e$  is the electron charge and we take the lattice constant “ $a$ ” to be about 4Å. A typical ME dielectric Fe<sub>3</sub>O<sub>4</sub> shows an electric polarization of  $\sim 1.0 \times 10^{-5}$  [C/m<sup>2</sup>] under an applied magnetic field  $H = 100$  [kOe]<sup>6</sup>. Compared with this, the ME effect discussed in this paper has 4 or 5 orders of magnitude larger (Sec. III). These electronic contribution to the ME effects can be hardly neglected compared with that of the displacement of the ligand anion atoms and so on, although the electronic contribution to the ME effects has been believed to be much smaller compared with the latters. This paper is organized as follows. In section II, we give our general idea for the magneto-electric effect based on its geometrical viewpoints. There we will explain how the flux and associated gauge field are introduced in the context of the spin dependent MEP. In section III, we propose two models which have nontrivial topological structure originated from the Dirac monopoles and exhibit a gigantic Magneto-Electronic response. These two models are independent of each other and can be read separately. Those who want to get the overview of this paper can skip this section. Section IV is devoted to conclusions.

## II. GEOMETRICAL VIEWPOINTS OF THE SPIN DEPENDENT MEP

### A. Macroscopic Electronic Polarization

In this article, we study the change of the electronic polarization which is induced when an perturbation  $\delta\hat{H}$  is added to the Hamiltonian  $\hat{H}$ , namely,  $\delta\vec{P}_{\text{el}} \equiv -\frac{e}{V}(\hat{X}_{\text{el}} - \langle\hat{X}_{\text{el}}\rangle_{\hat{H}})$ . Here  $\hat{X}_{\text{el}}$  is the sum of all the electron's position operators and  $V$  is the volume of the system.  $\langle\hat{X}_{\text{el}}\rangle_{\hat{H}}$  is the expectation value of  $\hat{X}_{\text{el}}$  before the perturbation is introduced. According to the Kubo formula for the linear response,  $\delta\vec{P}_{\text{el}} \equiv \langle\delta\vec{P}_{\text{el}}\rangle$  is given as

$$\delta\vec{P}_{\text{el}} = -i\frac{e}{V} \sum_{m \neq 0} \left( \frac{\langle\Psi_0|\hat{X}_{\text{el}}|\Psi_m\rangle\langle\Psi_m|\delta\hat{H}|\Psi_0\rangle}{(E_m - E_0)^2} - \text{c.c.} \right), \quad (3)$$

where  $\delta\hat{H} = i[\hat{H}, \delta\hat{H}]$  and  $|\Psi_m\rangle$  is an eigenstate of  $\hat{H}$  with an energy  $E_m$ . Here we assume the finite energy gap between the ground state  $|\Psi_0\rangle$  and the excited state  $|\Psi_m\rangle$  ( $m \geq 1$ ) and focus to the zero-temperature case.

When we transfer the time derivative from  $\delta\hat{H}$  to  $\hat{X}_{\text{el}}$ ,

$$\begin{aligned} & \langle\Psi_0|\hat{X}_{\text{el}}|\Psi_m\rangle\langle\Psi_m|[\hat{H}, \delta\hat{H}]\Psi_0\rangle \\ &= -\langle\Psi_0|[\hat{H}, \hat{X}_{\text{el}}]|\Psi_m\rangle\langle\Psi_m|\delta\hat{H}|\Psi_0\rangle \end{aligned} \quad (4)$$

we get

$$\delta\vec{P}_{\text{el}} = -\frac{i}{V} \sum_{m \neq 0} \left[ \frac{\langle\Psi_0|\hat{J}_{\text{el}}|\Psi_m\rangle\langle\Psi_m|\delta\hat{H}|\Psi_0\rangle}{(E_m - E_0)^2} - \text{c.c.} \right] \quad (5)$$

Here we introduced the electronic current operator,  $\vec{J}_{\text{el}} = -ie[\hat{H}, \hat{X}_{\text{el}}]$ . As shown in the appendix A, the change of the electronic polarization  $\delta\vec{P}_{\text{el}}$  can be also derived as the integrated electron current over the period during which the perturbation  $\delta H$  is introduced. Here the current operator  $\vec{J}_{\text{el}}$  is well defined on a periodic lattice, while the position operator  $\hat{X}_{\text{el}}$  is not. Thus, instead of eq.(3), we use eq.(5) as the change  $\delta\vec{P}_{\text{el}}$  of the electronic polarization. Let the Hamiltonian depend on an external parameter  $\vec{\varphi}$ , i.e.,  $\hat{H}(\vec{\varphi})$ . Then we can define a derivative of the electronic polarization  $\vec{P}_{\text{el}}$  with respect to  $\vec{\varphi}$  as

$$\frac{\partial\vec{P}_{\text{el}}}{\partial\varphi_\mu} = -\frac{i}{V} \sum_{m \neq 0} \left( \frac{\langle\Psi_0|\vec{J}_{\text{el}}|\Psi_m\rangle\langle\Psi_m|\frac{\partial\hat{H}}{\partial\varphi_\mu}|\Psi_0\rangle}{(E_m - E_0)^2} - \text{c.c.} \right). \quad (6)$$

Integrating eq.(6) with respect to  $\vec{\varphi}$  along a path  $\Gamma$ , the total change of the MEP,  $|\Delta_\Gamma\vec{P}_{\text{el}}|$ , can be also regarded as the total charges flowing through a unit area normal to  $\Delta_\Gamma\vec{P}_{\text{el}}$  after the adiabatic change along the path  $\Gamma$ .

### B. spin dependent MEP and the Flux

Now we study the spin dependent MEP. In this case, we identify the spin ordering field with  $\vec{\varphi}$  in the following way. At first we introduce an auxiliary field  $\vec{\phi}$  to Stratonovich-Hubbard decouple the on-site Coulomb repulsion and replace it by the saddle point solution as,

$$\begin{aligned} Z[\vec{h}] &\approx \int \mathcal{D}C^\dagger \mathcal{D}C \exp \left[ -\int L(\vec{\phi}_{\text{saddle point}}, C^\dagger, C, \vec{h}) \right] \\ &= \frac{U}{4} \sum_i |\vec{\phi}_{i,\text{saddle point}}|^2 + \sum_{i,\alpha} C_{i,\alpha}^\dagger (\partial_\tau - \mu) C_{i,\alpha} \\ &\quad - \sum_{i,j,\alpha} t_{ij} C_{i,\alpha}^\dagger C_{j,\alpha} + \frac{U}{2} \sum_{i,\alpha,\beta} \vec{\phi}_{i,\text{saddle point}} \cdot C_{i,\alpha}^\dagger [\vec{\sigma}]_{\alpha,\beta} C_{i,\beta} \\ &\quad + \vec{h} \cdot C_{i,\alpha}^\dagger [\vec{\sigma}]_{\alpha,\beta} C_{i,\beta}, \end{aligned}$$

where  $[\sigma_\nu]$  ( $\nu = x, y, z$ ) are the  $2 \times 2$  Pauli matrices. This saddle-point approximation corresponds to the mean field theory. Since this saddle-point solution is determined as a function of an applied magnetic field ( $\vec{h}$ ), we can control this spin ordering field by changing  $\vec{h}$ . We study the MEP induced by an adiabatic deformation of this spin ordering field  $\vec{\phi}_{i,\text{saddle point}}$ , which we will call simply  $\vec{\varphi}$  in the followings. When we consider a commensurate magnetic order, the wavefunction of an electronic state is given by the Slater determinant composed by the magnetic Bloch wavefunctions  $\langle\vec{R}_l, a, \mu, \alpha|\Phi_{n,\vec{k},\vec{\varphi}}\rangle = e^{i\vec{k}\cdot\vec{R}_l} \langle a, \mu, \alpha|n, \vec{k}, \vec{\varphi}\rangle$ , where  $\vec{R}_l$  represents the magnetic unit cell index and  $a, \mu, \alpha$  represent the sublattice, orbital and spin index, respectively. By using this single-particle magnetic Bloch wavefunction, the electric linear response given in eq.(6) reduces to a more compact form in terms of Thouless-Kohmoto-Nightingale-Nijs (TKNN) formula<sup>16</sup>,

$$\frac{\partial P_{\text{el},\mu}}{\partial\vec{\varphi}} \cdot \delta\vec{\varphi} = -ie \sum_{n:\text{VB}} \sum_{m:\text{CB}} \frac{1}{(2\pi)^d} \int_{\text{MBZ}} d\vec{k} \left( \frac{\langle n, \vec{k}, \vec{\varphi} | \frac{\partial H(\vec{k}, \vec{\varphi})}{\partial k_\mu} | m, \vec{k}, \vec{\varphi} \rangle \langle m, \vec{k}, \vec{\varphi} | \frac{\partial H(\vec{k}, \vec{\varphi})}{\partial \vec{\varphi}} | n, \vec{k}, \vec{\varphi} \rangle}{(\epsilon_m(\vec{k}, \vec{\varphi}) - \epsilon_n(\vec{k}, \vec{\varphi}))^2} - \text{c.c.} \right) \cdot \delta\vec{\varphi}$$

$$= -ie \sum_{n:\text{VB}} \frac{1}{(2\pi)^d} \int_{\text{MBZ}} d\vec{k} \left( \frac{\partial}{\partial k_\mu} \langle n, \vec{k}, \vec{\varphi} | \frac{\partial}{\partial \vec{\varphi}} | n, \vec{k}, \vec{\varphi} \rangle - \text{c.c.} \right) \cdot \delta\vec{\varphi}, \quad (7)$$

where  $H(\vec{k}, \vec{\varphi})$  is the Hamiltonian in the momentum representation and  $|n, \vec{k}, \vec{\varphi}\rangle$  is its eigenvector with eigenenergy  $\epsilon_n(\vec{k}, \vec{\varphi})$ . The inner products between  $\frac{\partial}{\partial k_\mu} |n, \vec{k}, \vec{\varphi}\rangle$  and  $\frac{\partial}{\partial \vec{\varphi}} |n, \vec{k}, \vec{\varphi}\rangle$  in the r.h.s. of eq.(7) is the contraction over sublattice, orbital and spin indice, i.e.,  $\sum_{a,\mu,\alpha} (\frac{\partial}{\partial k_\mu} \langle n, \vec{k}, \vec{\varphi} | a, \mu, \alpha \rangle) (\frac{\partial}{\partial \vec{\varphi}} \langle a, \mu, \alpha | n, \vec{k}, \vec{\varphi} \rangle)$ . Here the abbreviation 'CB', 'VB' and 'MBZ' represent the conduction bands, the valence bands and the magnetic Brillouin zone, respectively. When we take  $\vec{\varphi}$  as a two-component vector,  $\vec{\varphi} = (\varphi_1, \varphi_2)$ , and consider the one-dimensional system, the generalized momentum space is the three dimensional space spanned by the crystal momentum  $k$  and the external parameters  $\varphi_1$  and  $\varphi_2$ . In the following, the range of the magnetic Brillouin zone (MBZ) is denoted as  $[-\frac{\pi}{a_m}, \frac{\pi}{a_m}]$ , where  $a_m$  is the lattice constant of the magnetic unit cell (MUC). Here we can define the following vector fields for each energy band  $n$ .

$$\vec{\mathcal{B}}_n(k, \varphi_1, \varphi_2) = \vec{\nabla} \times \vec{\mathcal{A}}_n(k, \varphi_1, \varphi_2) \quad (8)$$

$$\vec{\mathcal{A}}_n(k, \varphi_1, \varphi_2) = -i \langle n, k, \varphi_1, \varphi_2 | \vec{\nabla} | n, k, \varphi_1, \varphi_2 \rangle \quad (9)$$

where  $\vec{\nabla} \equiv (\partial_k, \partial_{\varphi_1}, \partial_{\varphi_2})$ .

This vector field  $\vec{\mathcal{B}}_n(k, \varphi_1, \varphi_2)$  is independent of the U(1) gauge transformation of a magnetic Bloch wavefunction, i.e.,  $\langle \vec{R}_l, a, \mu, \alpha | \Phi_{n,k,\varphi_1,\varphi_2} \rangle \rightarrow e^{i\xi(k,\varphi_1,\varphi_2)} \langle \vec{R}_l, a, \mu, \alpha | \Phi_{n,k,\varphi_1,\varphi_2} \rangle$ , while  $\vec{\mathcal{A}}_n(k, \varphi_1, \varphi_2)$  changes by  $\vec{\nabla} \xi(k, \varphi_1, \varphi_2)$ . Thus we call  $\vec{\mathcal{B}}_n(k, \varphi_1, \varphi_2)$  and  $\vec{\mathcal{A}}_n(k, \varphi_1, \varphi_2)$  as the flux and gauge field, respectively. By using these vector fields, eq.(7) can be expressed as a surface integral of the flux over the rectangular surface spanned by  $\delta\vec{\varphi}$  and the  $k$ -axis, which is drawn as the shadowed region in Fig.1(a),

$$\frac{\partial P_{\text{el}}}{\partial \vec{\varphi}} \cdot \delta\vec{\varphi} = \frac{e}{2\pi} \sum_{n:\text{VB}} \int_{\delta\vec{\varphi} \times [-\frac{\pi}{a_m}, \frac{\pi}{a_m}]} d\vec{S} \cdot \vec{\mathcal{B}}_n(k, \varphi_1, \varphi_2) \quad (10)$$

Here the direction of  $d\vec{S}$  is taken so that  $\vec{n} - \delta\vec{\varphi} - d\vec{S}$  form the right-hand coordinates, where  $\vec{n}$  represents a unit vector along the  $k$ -axis, i.e.,  $\vec{n} = (1, 0, 0)$  as in Fig.1(a). Our strategy is (i) first to reveal the distribution of the flux for every filled energy band and then (ii) to determine the *optimal* direction,  $\delta\vec{\varphi}_{\text{opt}}$ , which maximize the magnetoelectric response given in eq.(10). For this purpose, we need to identify the *source* and/or *sink* of the flux, which we will discuss in the next subsection.

### C. Dirac monopole and Quantum Pump

When we deform  $\vec{\varphi}$  by a finite amount and put it back to the initial value  $\vec{\varphi}_i$ , i.e., making a loop  $\Gamma_{\text{cyc}}$  in the

$\varphi_1 - \varphi_2$  plane as in Fig.1(b), the total change of the electronic polarization induced by this process is the total flux penetrating the cylinder surface spanned by  $\Gamma_{\text{cyc}}$  and  $k$ -axis, i.e.,  $\Gamma_{\text{cyc}} \times [-\frac{\pi}{a_m}, \frac{\pi}{a_m}]$ ,

$$\begin{aligned} \Delta_{\text{cyc}} P_{\text{el}} &\equiv \oint_{\Gamma_{\text{cyc}}} \frac{\partial P_{\text{el}}}{\partial \vec{\varphi}} \cdot d\vec{\varphi} \\ &= \frac{e}{2\pi} \sum_{n:\text{VB}} \int_{\Gamma_{\text{cyc}} \times [-\frac{\pi}{a_m}, \frac{\pi}{a_m}]} d\vec{S} \cdot \vec{\mathcal{B}}_n. \end{aligned} \quad (11)$$

This is because the surface integrals of the flux  $\vec{\mathcal{B}}_n$  over the  $k = \frac{\pi}{a_m}$  plane and that over the  $k = -\frac{\pi}{a_m}$  plane cancel each other due to the periodicity. Thus if there are some sources and/or sinks of the flux of the filled bands inside this cylinder, we have a chance to obtain a non-zero change in the MEP after this cyclic deformation along  $\Gamma_{\text{cyc}}$ . This kind of the "d.c." response induced by the "a.c." impulse is called Quantum Pump<sup>11,12</sup>, since finite amounts of electrons are transported and/or *pumped* from the one-side to the other side of the system after one cycle of this adiabatic deformation. Since  $\vec{\nabla} \cdot \vec{\mathcal{B}}_n = \vec{\nabla} \cdot (\vec{\nabla} \times \vec{\mathcal{A}}_n) = 0$ , there are neither source nor sink associated with the flux  $\vec{\mathcal{B}}_n$  where the flux is well-defined, i.e., the  $n$ -th band is isolated from its neighboring bands. However in the region where the  $n$ -th band forms a degeneracy with its neighboring bands, the flux  $\vec{\mathcal{B}}_n$  become ill-defined. These degeneracy regions might become sources and/or sinks of the flux. As shown in the appendix B, when the  $n$ -th band and its neighboring band, say,  $(n+1)$ -th band form a doubly degenerate point at  $(k, \varphi_1, \varphi_2) = (k_D, \varphi_{1,D}, \varphi_{2,D})$ , this degenerate point becomes in general source and/or sink for the flux  $\vec{\mathcal{B}}_n$  (and also  $\vec{\mathcal{B}}_{n+1}$ ) with  $2\pi$  charge. We will call these doubly degenerate points as magnetic (anti-)monopoles or Dirac (anti-)monopoles from now on. Near this doubly degenerate point, the effective Hamiltonian for these two bands can be expanded in general as follows ,

$$\begin{aligned} [\mathbf{H}]_{2 \times 2}(k, \varphi_1, \varphi_2) &= (\epsilon_n(k_D, \varphi_{1,D}, \varphi_{2,D}) \\ &+ \vec{K} \cdot \vec{c})[\mathbf{1}] + \sum_{\mu,\nu} K_\mu V_{\nu,\mu} [\sigma_\nu], \end{aligned} \quad (12)$$

where  $\vec{K}$  is  $(k - k_D, \varphi_1 - \varphi_{1,D}, \varphi_2 - \varphi_{2,D})$ , and  $[\sigma_\nu]$  are the  $2 \times 2$  Pauli matrices. The vector  $\vec{c}$  is not important for our purpose, while the determinant of the  $3 \times 3$  matrix  $V$  plays an important role in classifying this degeneracy point. According to the appendix B, for the flux of the upper band,  $\vec{\mathcal{B}}_{n+1}(k, \vec{\varphi})$ , this degeneracy point acts as an anti-monopole (sink) in case of  $\det V < 0$ , while as a monopole (source) in case of  $\det V > 0$ . This relation is reversed for the flux for the lower band,  $\vec{\mathcal{B}}_n(k, \vec{\varphi})$ , i.e.,

$$\vec{\nabla} \cdot \vec{\mathcal{B}}_n = -2\pi \cdot \text{sign}(\det V) \delta^3(\vec{K}), \quad (13)$$

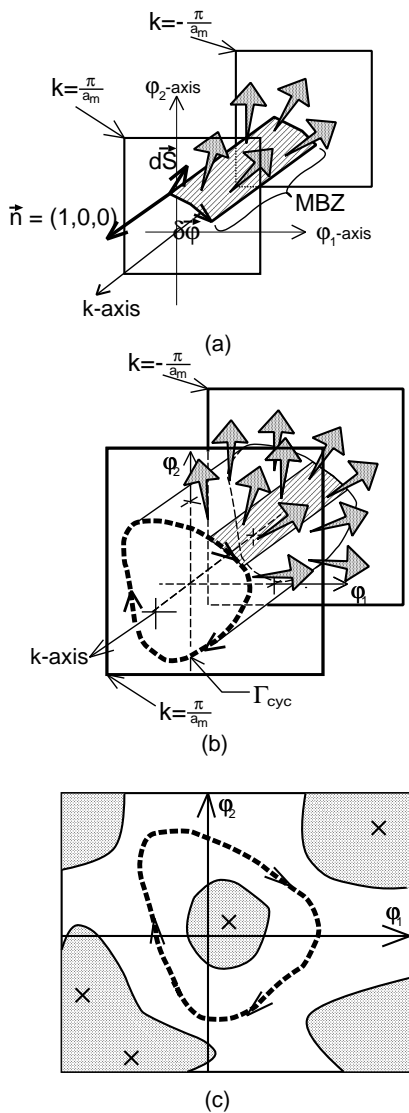


FIG. 1: (a) A shadowed rectangular area is subtended by  $\delta\vec{\varphi}$  and the line parallel to  $k$ -axis, i.e.,  $\delta\vec{\varphi} \times [-\frac{\pi}{a_m}, \frac{\pi}{a_m}]$ .  $\vec{n}$ ,  $\delta\vec{\varphi}$  and  $d\vec{S}$  form the right hand coordinates. The grey arrows represent the flux defined in eq.(8). (b) A cyclic deformation of the external parameters  $\vec{\varphi}$  in  $\varphi_1 - \varphi_2$  space. (c) Shaded regions are unphysical parameter regions in which the degenerate points (denoted by crossing points) are sometimes included. The MEP induced by the adiabatic change along the physical parameter line (denoted by broken line) is governed by the doubly degenerate points located in the shaded regions.

$$\vec{\nabla} \cdot \vec{\mathcal{B}}_{n+1} = 2\pi \cdot \text{sign}(\det V) \delta^3(\vec{K}). \quad (14)$$

Thus when we fill both of these two bands by electrons, roughly speaking,  $\vec{\mathcal{B}}_n(k, \vec{\varphi})$  and  $\vec{\mathcal{B}}_{n+1}(k, \vec{\varphi})$  cancel each other in the summation of the r.h.s. of eq.(10) and the degeneracy point between the  $n$ -th and  $(n+1)$ -th band is irrelevant for the MEP. On the other hand, when only the lower band is filled by electrons,  $\vec{\mathcal{B}}_n(k, \vec{\varphi})$  contributes to the MEP without being cancelled by its

counter part  $\vec{\mathcal{B}}_{n+1}(k, \vec{\varphi})$  and results in a gigantic linear response, where the doubly degenerate point between these two bands plays an essential role in the direction and magnitude of the MEP. Those ME dielectrics which belong to the latter case of the electron filling are good candidates where this mechanism becomes relevant. When we turn to the Quantum Pump, the sign change between eq.(13) and eq.(14) simplifies eq.(11) and gives us more intuitive form. When both the  $(n+1)$ -th and  $n$ -th bands are filled, a pair of magnetic monopole(anti-monopole) for the  $(n+1)$ -th band and anti-monopole(monopole) for the  $n$ -th band cancel each other in the summation of the r.h.s. of eq.(11). Thus the degeneracy points between filled bands do not contribute to the  $\Delta_{\text{cyc}} P_{\text{el}}$  in eq.(11) and a finite  $\Delta_{\Gamma_{\text{cyc}}} P_{\text{el}}$  is originated only from the degeneracy points where the highest valence band (HVB) and the lowest conduction band (LCB) touch. As a result, we obtain

$$\Delta_{\text{cyc}} P_{\text{el}} = -e \times \sum_{i=1}^N \text{sign}(\det V_i), \quad (15)$$

where the index  $i$  represents the doubly degenerate points between the HVB and the LCB.  $N$  is the total number of these degenerate points. The  $3 \times 3$  matrix  $V$  given in eq.(12) is defined for each doubly degenerate point and we refer to that of  $i$ -th point as  $V_i$ . If the path  $\Gamma_{\text{cyc}}$  is contractible into one point without confronting the metallic region where the HVB and the LCB form a band crossing,  $\Delta_{\Gamma_{\text{cyc}}} P_{\text{el}}$  should be zero. And eq.(15) means that the path  $\Gamma_{\text{cyc}}$  must be at least noncontractible, in order to get non-zero  $\Delta_{\Gamma_{\text{cyc}}} P_{\text{el}}$ . When we fix the electron number per site, the parameter values at which the HVB and the LCB form doubly degenerate points are unphysical points and these degeneracies are lifted in general at those parameter points which are physically realized (saddle points). What is important and nontrivial is that the MEP induced by the adiabatic change in these gapped phase is controlled by the doubly degenerate points hidden in its neighboring unphysical parameter points (See Fig.1(c)).

As is evident from eq.(12), we need to tune only 3 real-valued parameters in order to lift the double degeneracy. Thus when we add another parameter  $\varphi_{\text{perturb}}$  and constitute a four dimensional parameter space, the double degeneracy occurs on a line in this 4D space. As a result, these magnetic (anti)monopoles are stable against small perturbations. This is similar to the stability of the integer quantum Hall insulator against small perturbations.

### III. GIGANTIC ME EFFECT

Based on the concept developed in the section II, we construct some particular models showing a gigantic ME effect. In the first model, the MEP is attributed to the screw spin structures, while it is due to the spin-orbit coupling in the second model. We consider only the 1D case

in the former model, while, in the latter one, we generalize it into the 2D case by introducing a weak interchain coupling. The generalization of the 1D case into higher dimensions is justified since the magnetic (anti)monopoles are stable against a small perturbations.

### A. screw spin structure

We consider the following 1D system with the screw spin structure of three sublattices in a MUC as shown in Fig.2(a),

$$\begin{aligned} \hat{H} = & t \sum_{l,\alpha} (C_{l,1,\alpha}^\dagger C_{l,2,\alpha} + C_{l,2,\alpha}^\dagger C_{l,3,\alpha} + C_{l,3,\alpha}^\dagger C_{l+1,1,\alpha}) \\ & + t' \sum_{l,\alpha} (C_{l,1,\alpha}^\dagger C_{l,3,\alpha} + C_{l,2,\alpha}^\dagger C_{l+1,1,\alpha} + C_{l,3,\alpha}^\dagger C_{l+1,2,\alpha}) \\ & + \text{c.c.} \\ & + \frac{U}{2} \sum_{l,\alpha,\beta} (\vec{\varphi}_1 \cdot C_{l,1,\alpha}^\dagger [\vec{\sigma}]_{\alpha,\beta} C_{l,1,\beta} \vec{\varphi}_2 \cdot C_{l,2,\alpha}^\dagger [\vec{\sigma}]_{\alpha,\beta} C_{l,2,\beta} \end{aligned}$$

$$+ \vec{\varphi}_3 \cdot C_{l,3,\alpha}^\dagger [\vec{\sigma}]_{\alpha,\beta} C_{l,3,\beta}) \quad (16)$$

$$\text{where } \vec{\varphi}_i = (\sin \theta_i \cos \phi_i, \sin \theta_i \sin \phi_i, \cos \theta_i) \quad (17)$$

where  $t$  and  $t'$  are the transfer integrals between the nearest and the next nearest neighbor sites. Here the spatial inversion symmetry is broken by this screw spin structure. There are six bands; 3 upper Hubbard bands (UHB) and 3 lower Hubbard bands (LHB). In the following, we study the MEP induced by an adiabatic deformation of  $\vec{\varphi}_3$  when the lower 2 bands of LHB are filled by electrons, i.e., 2 electrons per single MUC.

When we take the infinite  $U$  limit, we can map the above Hamiltonian into the spinless fermion model, i.e., the effective Hamiltonian for the LHB. By taking the Fourier transformation,  $f_{k,j}^\dagger = \frac{1}{N} \sum_l f_{l,j}^\dagger e^{-ik \cdot (3l+j)a}$  (“ $a$ ” is the lattice constant and  $l,j$  denotes the MUC index and sublattice index respectively), this spinless Hamiltonian is given in the momentum representation as  $\hat{H}_{\text{spinless}} = \sum_{i,j=1}^3 \sum_k [H(k)]_{i,j} f_{k,i}^\dagger f_{k,j}$ , where

$$[H(k)] = |T(k)| \begin{bmatrix} 0 & \cos(\frac{\theta_{12}}{2}) e^{-ia_{12}} e^{i\phi_t(k)} & \cos(\frac{\theta_{13}}{2}) e^{-ia_{13}} e^{-i\phi_t(k)} \\ \cos(\frac{\theta_{12}}{2}) e^{ia_{12}} e^{-i\phi_t(k)} & 0 & \cos(\frac{\theta_{23}}{2}) e^{-ia_{23}} e^{i\phi_t(k)} \\ \cos(\frac{\theta_{13}}{2}) e^{ia_{13}} e^{i\phi_t(k)} & \cos(\frac{\theta_{23}}{2}) e^{ia_{23}} e^{-i\phi_t(k)} & 0 \end{bmatrix}. \quad (18)$$

Here  $|T(k)|$  and  $\phi_t(k)$  are the amplitude and the argument of the complex number  $te^{-ika} + t'e^{i2ka}$ , where  $k$  is the crystal momentum and the MBZ is  $[-\frac{\pi}{3a}, \frac{\pi}{3a}]$ .  $\theta_{ij}$  is the relative angle between spin  $\vec{\varphi}_i$  and  $\vec{\varphi}_j$ . The phase factor  $e^{ia_{ij}}$  is accompanied when an electron hops from a site in the  $i$ -sublattice to another site in the  $j$ -sublattice, which depends on the gauge choice of  $f_{l,i}^\dagger$ . On the other hand,  $a_{12} + a_{23} + a_{31} \equiv \Phi$  is one half of the solid angle subtended by  $\vec{\varphi}_1, \vec{\varphi}_2, \vec{\varphi}_3$  and independent of the gauge choice. In the following, we will show first the analytic results in case of  $t' = 0$ . The situation does not change essentially even in case of finite  $t'$ . As mentioned in section II, the MEP in an insulating phase is controlled by the level crossing point in its neighboring metallic phase. Thus we first examine the case where the direct gap between the HVB ( $n = 2$ ) and the LCB ( $n = 3$ ) closes and the system becomes metallic. According to the secular equation for this effective Hamiltonian, i.e.,  $-\lambda^3 + (\cos(\frac{\theta_{12}}{2})^2 + \cos(\frac{\theta_{23}}{2})^2 + \cos(\frac{\theta_{31}}{2})^2)\lambda + 2 \cos(\frac{\theta_{12}}{2}) \cos(\frac{\theta_{23}}{2}) \cos(\frac{\theta_{31}}{2}) \cos(-\Phi + 3\phi_t(k)) = 0$ , the HVB and LCB form doubly degenerate points at  $k = \phi_t^{-1}(\frac{(2n+1)\pi}{3} + \frac{\Phi}{3}) = -\frac{1}{a}(\frac{(2n+1)\pi}{3} + \frac{\Phi}{3})$ , when  $\vec{\varphi}_1, \vec{\varphi}_2, \vec{\varphi}_3$  form a regular triangle, i.e.,  $\cos(\frac{\theta_{12}}{2}) = \cos(\frac{\theta_{23}}{2}) = \cos(\frac{\theta_{31}}{2})$ . This is natural because the lattice periodicity reduces from “ $3a$ ” to “ $a$ ” in this case. When we fix  $\vec{\varphi}_1$  and  $\vec{\varphi}_2$  at first, there are two ways of making a regular triangle as shown in Fig.2(b). One way is to form a regu-

lar triangle with  $\Phi \equiv \Phi_0 > 0$  ( $\vec{\varphi}_3 = \vec{\varphi}_{3,m}$ ) and the other is that with  $\Phi_0 < 0$  ( $\vec{\varphi}_3 = \vec{\varphi}_{3,am}$ ). In the former case, a degeneracy point appears at  $k = -\frac{1}{a}(-\frac{\pi}{3} + \frac{|\Phi_0|}{3})$  within the MBZ, while at  $k = -\frac{1}{a}(\frac{\pi}{3} - \frac{|\Phi_0|}{3})$  in the latter case. When we deform  $\vec{\varphi}_3$  from the apexes of these regular triangles ( $\vec{\varphi}_3 \neq \vec{\varphi}_{3,m}, \vec{\varphi}_{3,am}$ ), these doubly degenerate points are lifted and the band gap between the HVB and LCB appears as in Fig.2(c). Then the HVB and the LCB form two doubly degenerate points in the 3D parameter space subtended by  $k$  and  $\vec{\varphi}_3$  as shown in Fig.3(a). In Fig.3(a), we draw two spheres whose radii are  $R$  and  $R + \frac{2\pi}{3a}$ . We regard the spherical shell, which is sandwiched by these two spheres, as the  $k - \vec{\varphi}_3$  space. Namely, we identify  $(k, \vec{\varphi}_3)$  with the point,  $(x, y, z) \equiv (R + k + \frac{\pi}{3a})\vec{\varphi}_3$  in Fig.3(a) and the above two doubly degenerate points are identified with

$$(x, y, z) = \begin{cases} (R + \frac{|\Phi_0|}{3a})\vec{\varphi}_{3,am} & \text{for } -\pi < \Phi_0 < 0, \\ (R + \frac{2\pi}{3a} - \frac{|\Phi_0|}{3a})\vec{\varphi}_{3,m} & \text{for } 0 < \Phi_0 < \pi. \end{cases} \quad (19)$$

Here we should mention that we have a periodic boundary condition along the radial direction, i.e.,  $H(R\vec{\varphi}_3) = H((R + \frac{2\pi}{3a})\vec{\varphi}_3)$  and we regard  $R\vec{\varphi}_3$  and  $(R + \frac{2\pi}{3a})\vec{\varphi}_3$  as the identical points. As was explained in section II, these doubly degenerate points in the 3D parameter space become in general magnetic monopoles (source) and/or anti-monopoles (sink) for the flux  $\vec{B}_{\text{HVB}}$  ( $\vec{B}_{\text{LCB}}$ ) defined

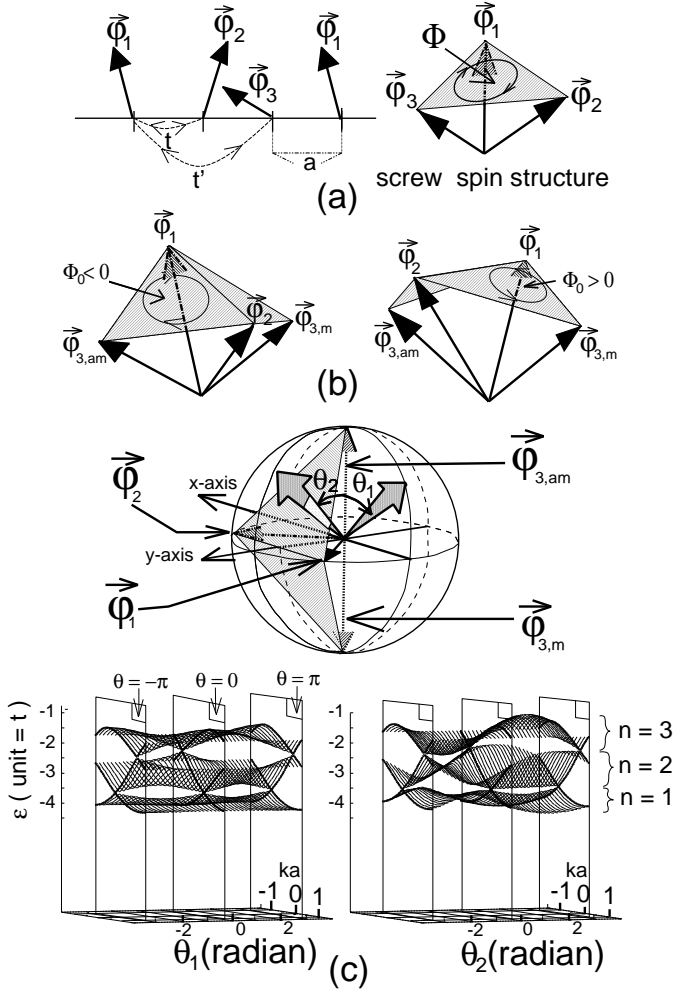


FIG. 2: (a) A screw spin structure with 3 sublattices. (b)  $\vec{\varphi}_1, \vec{\varphi}_2$  and  $\vec{\varphi}_{3,m}$  subtend a regular triangle with  $\Phi_0 > 0$  while  $\vec{\varphi}_1, \vec{\varphi}_2$  and  $\vec{\varphi}_{3,am}$  subtend one with  $\Phi_0 < 0$ . (c) An energy dispersion for the lower three bands (LHB) in case of  $\theta_{12} = \frac{\pi}{2}$  as a function of  $\varphi_3$  and the crystal momentum  $k$ . The doubly degenerate points between the HVB ( $n=2$ ) and the LCB ( $n=3$ ) are lifted when the  $\vec{\varphi}_3$  is departed from the apexes of the regular triangles in (b), i.e.,  $\theta \neq 0, \pm\pi$

as,

$$\vec{B}_n(x, y, z) = -i\vec{\nabla} \times \langle n, x, y, z | \vec{\nabla} | n, x, y, z \rangle,$$

$$\vec{\nabla} = \left( \frac{\partial}{\partial x}, \frac{\partial}{\partial y}, \frac{\partial}{\partial z} \right).$$

When we expand eq.(18) around these degeneracy points and make the  $2 \times 2$  Hamiltonian for the HVB and the LCB as in eq.(12), we can calculate the sign of their magnetic charges as

$$\text{sign}(\det V) = \begin{cases} 0, & \text{for } \Phi_0 = -\pi \\ 1, & \text{for } -\pi < \Phi_0 < 0 \\ 0, & \text{for } \Phi_0 = 0 \\ -1, & \text{for } 0 < \Phi_0 < \pi \\ 0, & \text{for } \Phi_0 = \pi \end{cases} \quad (20)$$

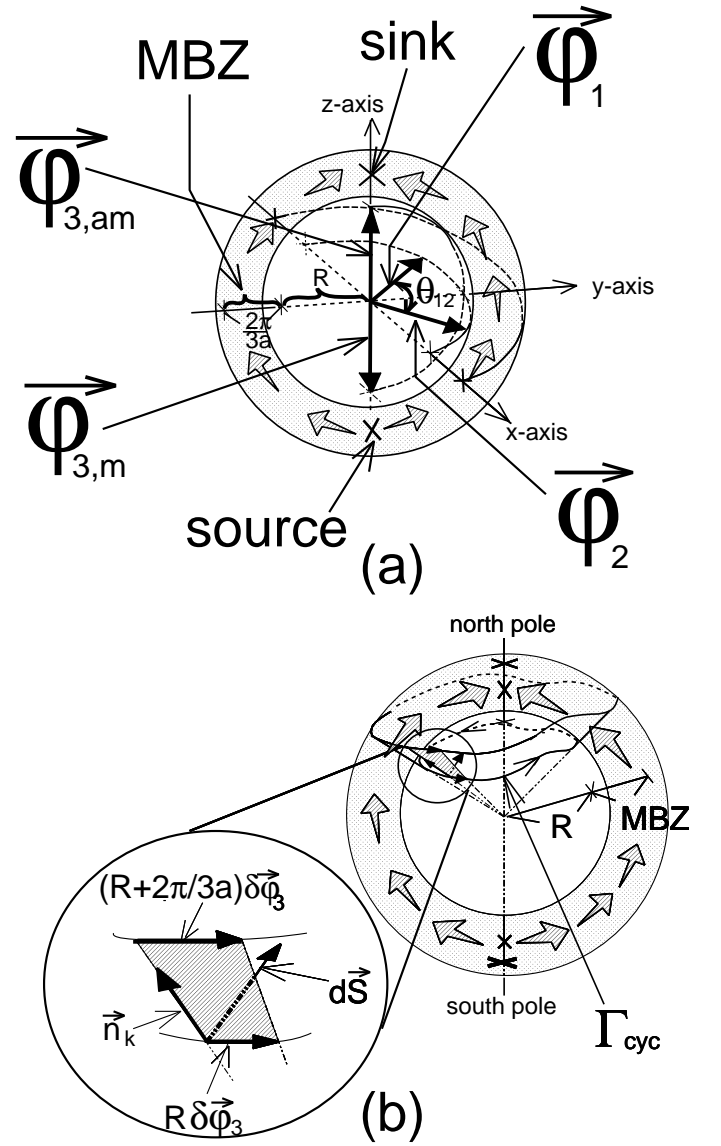


FIG. 3: (a) A parameter space ( $k - \vec{\varphi}_3$  space) is the spherical shell region (the dotted region) with its width  $\frac{2\pi}{3a}$ , i.e.,  $(x, y, z) = \{(R + k + \frac{\pi}{3a})\vec{\varphi}_3 | -\frac{\pi}{3a} \leq k \leq \frac{\pi}{3a}, |\vec{\varphi}_3| = 1\}$ . Here  $R$  is an arbitrary positive constant, which we introduce just for visibility. The flux  $\vec{B}_{n=2}$  (shaded arrows) streams from its source at  $(R + \frac{2\pi}{3a} - \frac{|\Phi_0|}{3a})\vec{\varphi}_{3,m}$  and sinks into the points at  $(R + \frac{|\Phi_0|}{3a})\vec{\varphi}_{3,am}$ . (b) A surface integral of the flux  $\vec{B} = \sum_{n:VB} \vec{B}_n$  (whose distribution is given in Fig.4) over the shaded (zoomed-up) region is the MEP accompanied by the adiabatic deformation  $\delta\vec{\varphi}_3$ .

Thus the doubly degenerate point at  $(R + \frac{|\Phi_0|}{3a})\vec{\varphi}_{3,am}$  is an anti-monopole (sink) for the flux  $\vec{B}_{n=2}$  while  $(R + \frac{2\pi}{3a} - \frac{|\Phi_0|}{3a})\vec{\varphi}_{3,m}$  is a monopole (source) for the flux  $\vec{B}_{n=2}$  as shown in Fig.3(a). Since the  $k - \vec{\varphi}_3$  space is compact, this pair of monopole and anti-monopole is nothing but the so-called species doubling<sup>17</sup>. These magnetic (anti)monopoles are stable against small perturba-

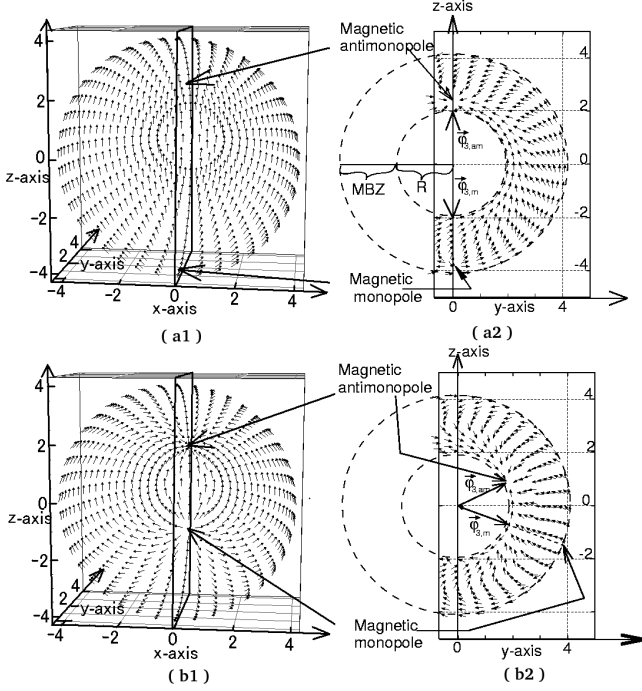


FIG. 4: A distribution of the flux  $\vec{B}_{1+2} \equiv \sum_{n=1,2} \vec{B}_n$  on the  $k - \vec{\varphi}_3$  space, where  $(x, y, z) = (R + k + \frac{\pi}{3a})\vec{\varphi}_3$ . Here we draw their distribution in the range  $y > 0$  for visibility. The magnitudes of the vectors are normalized to be the same in order to show only their direction. In this calculation, the two vectors  $\vec{\varphi}_1$  and  $\vec{\varphi}_2$  are in the  $x$ - $y$ -plane, i.e.,  $\theta_1 = \theta_2 = \frac{\pi}{2}$  and  $\phi_1 = \frac{\pi}{2} + \frac{\theta_{12}}{2}$ ,  $\phi_2 = \frac{\pi}{2} - \frac{\theta_{12}}{2}$  in eq.(17), and the relative angle  $\theta_{12}$  between these two vectors is taken to be  $\frac{\pi}{2}$  in Fig.(a1),(a2) and  $\frac{\pi}{7}$  in Fig.(b1),(b2). We take  $t = 1.0$ ,  $t' = 0.1$ ,  $U = 5.0$ ,  $R = 3.0$ ,  $a = 1$ . In Fig.(a1) and (b1), we draw the distribution of the flux  $\vec{B}_{1+2}$  on the  $k = \frac{\pi}{3a}(|(x, y, z)| = R + \frac{\pi}{3a})$  sphere. In Fig.(a2) and (b2) we draw their distribution on the  $x = 0$  plane where  $x$ -component of the flux always vanishes. On this plane, there is a pair of its source and sink. In Fig.(b1) and (b2), a pair of the source and sink move toward the equator in comparison with Fig.(a1) and (a2).

tions. For example, they remain essentially unchanged even when  $U$  and  $t'$  are finite. In Fig.4, we show the distribution of the flux  $\vec{B}_{1+2} = \vec{B}_1 + \vec{B}_2$  calculated numerically with finite  $U$  and  $t'$ . In this calculation, the two vectors  $\vec{\varphi}_1$  and  $\vec{\varphi}_2$  are confined in the  $x$ - $y$ -plane, i.e.,  $\theta_1 = \theta_2 = \frac{\pi}{2}$  and  $\phi_1 = \frac{\pi}{2} + \frac{\theta_{12}}{2}$ ,  $\phi_2 = \frac{\pi}{2} - \frac{\theta_{12}}{2}$  in eq.(17) with the relative angle  $\theta_{12}$  between these two vectors being  $\frac{\pi}{2}$  (Fig.4(a1),(a2)) and  $\frac{\pi}{7}$  (Fig.4(b1),(b2)), respectively.

In the first case (Fig.4(a1),(a2)), we found a sink of the flux  $\vec{B}_{1+2}$  on the north pole ( $\theta_3 = 0$ ) and a source on the south pole ( $\theta_3 = \pi$ ) directions. The flux streaming from the source flows upward until it sinks into the sink in the north as shown in Fig.4(a1),(a2). These source and sink are nothing but the magnetic monopole and anti-monopole of the flux  $\vec{B}_2$ . The source on the south pole direction corresponds to  $0 < \Phi_0 < \pi$ , while the sink on

the north pole direction corresponds to  $-\pi < \Phi_0 < 0$  in eqs.(19),(20). In the second case (Fig.4(b1),(b2)), where the relative angle  $\theta_{12}$  becomes smaller than  $\frac{\pi}{2}$ , this pair of source and sink moves toward the equator gradually. Finally they merge into a single point on the equator when the  $\vec{\varphi}_1$  and  $\vec{\varphi}_2$  become parallel. This corresponds to  $\Phi_0 = 0$ ,  $\vec{\varphi}_{3,m} = \vec{\varphi}_{3,am}$  in eqs.(19),(20).

In this spherical shell picture, the dielectric response with respect to an adiabatic deformation  $\delta\vec{\varphi}_3$  is given by the surface integral of the flux  $\vec{B}_{1+2}$  over the rectangular subtended by the two vectors,  $R\delta\vec{\varphi}_3$  and  $(R + \frac{2\pi}{3a})\delta\vec{\varphi}_3$  in Fig.3(b), namely,  $\int_{\text{the shadowed region in Fig.3(b)}} d\vec{S} \cdot \vec{B}_{1+2}$ , where  $\vec{n}_k - \delta\vec{\varphi}_3 - d\vec{S}$  form the right-hand coordinates. Thus, when we deform  $\vec{\varphi}_3$  adiabatically around the north pole anticlockwise, i.e., along the  $\Gamma_{\text{cyc}}$  in Fig.3(b), and get it back to its initial value, the electronic polarization increases by  $e$  in case of  $\theta_{12} = \frac{\pi}{2}$  (Fig.4(a1),(a2)). This quantized value remains invariant even though  $\theta_{12}$  deviates slightly from  $\frac{\pi}{2}$ . However,  $\Delta_{\Gamma_{\text{cyc}}} P_{\text{el}}$  becomes zero, when  $\theta_{12}$  changes so that the magnetic antimonopole of the flux  $\vec{B}_2$  moves outside the cylinder;  $\Gamma_{\text{cyc}} \times [R, R + \frac{2\pi}{3a}]^{18}$ .

## B. spin-orbit coupling

We next consider another model where the *global* rotation in a spin space induces a gigantic electronic polarization. In this case, the spin-orbit coupling plays a crucial role, because the global rotation in the spin space cannot change the solid angle subtended by several spins.

Let's consider an antiferromagnet where the sublattice magnetizations collinear to a particular direction  $\vec{\varphi}_{\text{AF}}$  are canted by a magnetic field applied perpendicular to this direction, resulting in a finite net magnetization  $\vec{M}_{\perp}$  as shown in Fig.5(a). We can control the direction and magnitude of this ferromagnetic moment  $\vec{M}_{\perp}$  by using the applied magnetic field. The hopping integral between orbitals on the nearest neighbor sites depends on the intermediate anion ions, for example, oxygen  $\text{O}^{2-}$ . In Fig.5(b), we introduce the uniform shifts of oxygen atoms along the  $x$ -direction, since our spin structure itself does not break the spatial inversion symmetry.

By adding an orbital index on each site in the tight binding model, we study the dielectric property of a model composed of the d-orbitals with the spin-orbit interaction and the antiferromagnetic order. At first, we give the result of the 1-dimensional system extending along the  $y$ -direction (bold line in Fig.5(b)). Next we give the 2-dimensional generalization by adding the electron transfer along the  $x$ -direction.

The crystal field term and the kinetic energy of the 1-dimensional system extending along the  $y$ -direction are given as follows.

$$H_{K,y\text{-direction}} = \sum_{i_y, \mu, \nu, \alpha} C_{i_y + a_y, \mu, \alpha}^{\dagger} [t^y]_{\mu, \nu} C_{i_y, \nu, \alpha} + \text{c.c.}$$

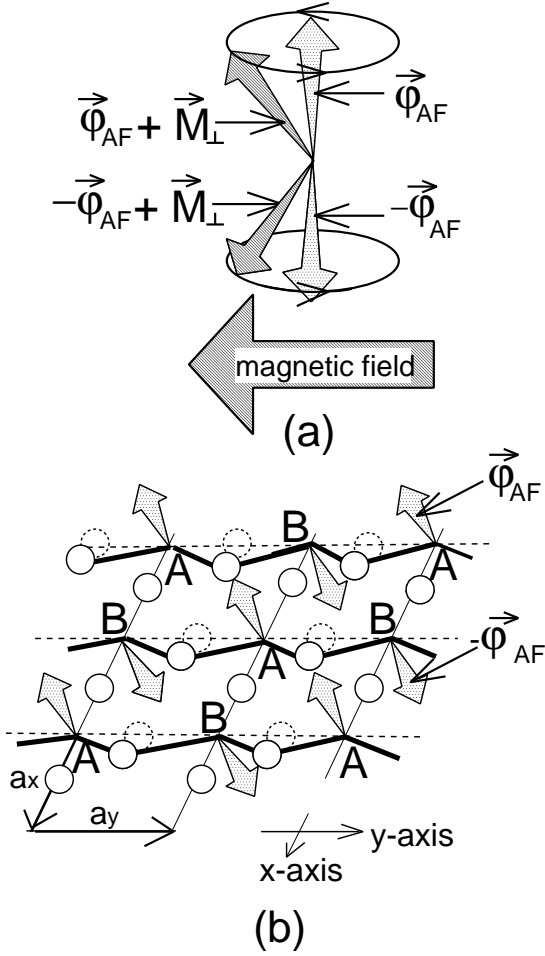


FIG. 5: (a) An applied magnetic field cants the sublattice magnetizations and produces the ferromagnetic moment  $\vec{M}_\perp$ . Thus the sublattice magnetization  $\vec{\varphi}_{AF} + \vec{M}_\perp$  is for the A-sublattice, while  $-\vec{\varphi}_{AF} + \vec{M}_\perp$  is for B-sublattice, where A- and B-sublattice are defined in Fig.(b). We take the  $M_{\perp,x}$ -axis and  $M_{\perp,y}$ -axis as  $(\cos \theta \cos \phi, \cos \theta \sin \phi, -\sin \theta)$  and  $(-\sin \phi, \cos \phi, 0)$  respectively, where  $\vec{\varphi}_{AF} = (\sin \theta \cos \phi, \sin \theta \sin \phi, \cos \theta)$ . (b) A modulated square lattice with the staggered magnetization on A- and B-sublattice. White circles denote the anion atoms ( $O^{2-}$ ) while the transition metal atoms are located on the lattice. Here we draw the 1D chains extending along the  $y$ -direction as bold lines, while the interchain couplings are introduced as thin lines. Here the anion atoms on the 1D chain is shifted along the  $x$ -direction uniformly.

$$H_{CF} = \sum_{i_y, \mu, \alpha} \epsilon_\mu C_{i_y, \mu, \alpha}^\dagger C_{i_y, \mu, \alpha}$$

$$\text{where } [\mathbf{t}^y] = [\mathbf{t}^{y,s}] + [\mathbf{t}^{y,a}]$$

$$= \begin{bmatrix} -t_0 & -t_1 & 0 & 0 & 0 \\ -t_1 & -t_2 & 0 & 0 & 0 \\ 0 & 0 & -t_5 & 0 & 0 \\ 0 & 0 & 0 & -t_5 & 0 \\ 0 & 0 & 0 & 0 & 0 \end{bmatrix}$$

$$+ \begin{bmatrix} 0 & 0 & -t_3 & 0 & 0 \\ 0 & 0 & -t_4 & 0 & 0 \\ t_3 & t_4 & 0 & 0 & 0 \\ 0 & 0 & 0 & 0 & t_6 \\ 0 & 0 & 0 & -t_6 & 0 \end{bmatrix}. \quad (21)$$

Here the first term is the crystal field and  $\epsilon_\mu$  is the energy of the orbital  $\mu = d_{x^2-y^2}, d_{3z^2-r^2}, d_{xy}, d_{yz}, d_{zx}$ . The transfer integrals are composed of the symmetric parts  $[\mathbf{t}^{y,s}]$  and antisymmetric parts  $[\mathbf{t}^{y,a}]$ . The antisymmetric transfer integrals  $t_3, t_4, t_6$  result from the oxygen ions' shifts and their signs are reversed when the oxygen ions slide in the opposite direction ( $-x$  direction). Thus these transfer integrals break the spatial inversion symmetry  $I$ . Also  $t_1$  is induced by the displacement of the oxygen ions. Here the on-site spin-orbit coupling is introduced as

$$H_{LS} = \sum_{\alpha, \beta, \mu, \nu} \lambda C_{i, \mu, \alpha}^\dagger [\vec{L}]_{\mu, \nu} \cdot [\vec{\sigma}]_{\alpha, \beta} C_{i, \nu, \beta},$$

$$\text{where } [\mathbf{L}_x] = \begin{bmatrix} 0 & 0 & 0 & -i & 0 \\ 0 & 0 & 0 & -\sqrt{3}i & 0 \\ 0 & 0 & 0 & 0 & i \\ i & \sqrt{3} & 0 & 0 & 0 \\ 0 & 0 & -i & 0 & 0 \end{bmatrix},$$

$$[\mathbf{L}_y] = \begin{bmatrix} 0 & 0 & 0 & 0 & i \\ 0 & 0 & 0 & 0 & -\sqrt{3}i \\ 0 & 0 & 0 & i & 0 \\ 0 & 0 & -i & 0 & 0 \\ -i & \sqrt{3}i & 0 & 0 & 0 \end{bmatrix},$$

$$[\mathbf{L}_z] = \begin{bmatrix} 0 & 0 & 2i & 0 & 0 \\ 0 & 0 & 0 & 0 & 0 \\ -2i & 0 & 0 & 0 & 0 \\ 0 & 0 & 0 & 0 & -i \\ 0 & 0 & 0 & i & 0 \end{bmatrix}. \quad (22)$$

In a similar way as before, we introduce the coupling between the staggered magnetic moment and the electrons as

$$\frac{U}{2} \sum_{i, \mu, \alpha, \beta} \vec{\varphi}_i \cdot C_{i, \mu, \alpha}^\dagger [\vec{\sigma}]_{\alpha, \beta} C_{i, \mu, \beta}, \quad (23)$$

$$\text{where } \begin{cases} \vec{\varphi}_i = \vec{\varphi}_{AF} + \vec{M}_\perp & i \text{ is on A-sublattice} \\ \vec{\varphi}_i = -\vec{\varphi}_{AF} + \vec{M}_\perp & i \text{ is on B-sublattice.} \end{cases}$$

The two-component ferromagnetic moment  $\vec{M}_\perp = (M_{\perp,x}, M_{\perp,y})$  can be controlled by the applied magnetic field. Then we interpret  $\vec{\nabla}$  in eq.(8) as  $(\frac{\partial}{\partial M_{\perp,x}}, \frac{\partial}{\partial M_{\perp,y}}, \frac{\partial}{\partial k_y})$  and calculate the distribution of the flux  $\vec{B}_n(\vec{M}_\perp, k_y)$  for each energy band  $n$ . Here  $k_y$  is the crystal momentum of this 1D system and its MBZ is taken as  $[-\frac{\pi}{2a_y}, \frac{\pi}{2a_y}]$ . Then, by summing the flux over the band indices up to the HVB, the distribution of  $\vec{B}(\vec{M}_\perp, k_y) = \sum_{n: \text{VB}} \vec{B}_n(\vec{M}_\perp, k_y)$  in the  $M_{\perp,x} - M_{\perp,y} - k_y$  space is obtained as shown in Fig.6, where the lower 3 bands are filled by electrons. The HVB ( $n = 3$ ) is mainly composed of  $xy$ -orbitals at A-site and B-site.

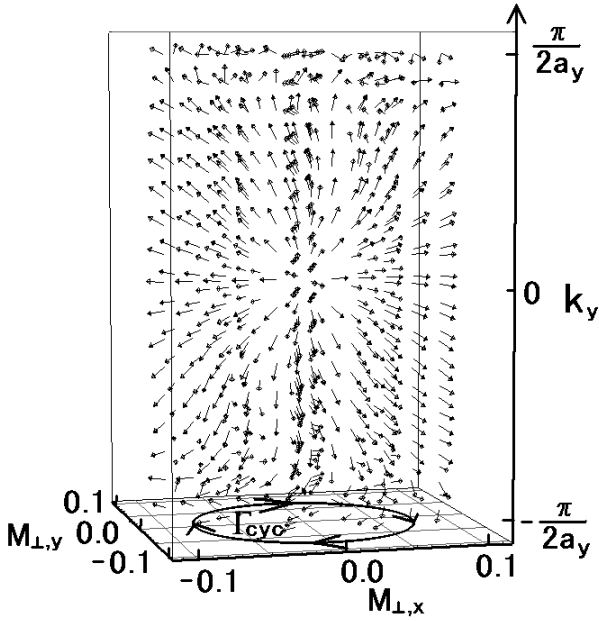


FIG. 6: A distribution of the flux  $\sum_{n=1}^3 \vec{B}_n$ . Here  $\frac{t_0}{U} = 0.125$ ,  $\frac{t_1}{U} = 0.1$ ,  $\frac{t_2}{U} = 0.025$ ,  $\frac{t_3}{U} = 0.075$ ,  $\frac{t_4}{U}, \frac{t_5}{U}, \frac{t_6}{U} = 0.05$ ,  $\frac{\lambda}{U} = 0.025$ ,  $\frac{\epsilon_{x^2-y^2}}{U} = 1.25$ ,  $\frac{\epsilon_{3z^2-r^2}}{U} = 1.3$ ,  $\frac{\epsilon_{xy}}{U} = 0.05$ ,  $\frac{\epsilon_{yz}}{U} = 0.0$ ,  $\frac{\epsilon_{zx}}{U} = 0.05$ ,  $\vec{\varphi}_{AF} \parallel [1, 1, 1]$  and  $|\vec{\varphi}_{AF}| = 1$ . The vertical axis of this figure is the  $k_y$ -axis whose range is taken to be  $[-\frac{\pi}{2a_y}, \frac{\pi}{2a_y}]$  and we take  $a_y = 10$  for visibility. The magnitudes of the vectors are normalized to be the same in order to show only their direction.

From Fig.5, it is naturally understood that the system with  $\vec{M}_\perp$  can be transformed into that with  $-\vec{M}_\perp$  by the time-reversal operator  $\{R|a_y\}$ . Here  $\{R|a_y\}$  represents the time-reversal operation followed by the spatial translation by the lattice constant  $a_y$ , which exchanges A and B sublattices. Thus the magnetic Bloch wave function  $\langle \vec{R}_l, a, \mu, \alpha | \Phi_{n, \vec{k}, \vec{\varphi}} \rangle = e^{i\vec{k} \cdot \vec{R}_l} \langle a, \mu, \alpha | n, \vec{k}, \vec{\varphi} \rangle$  obeys

$$\langle a, \mu, \alpha | n, k, \vec{M}_\perp \rangle = \sum_{b, \beta} \begin{bmatrix} 0 & 1 \\ 1 & 0 \end{bmatrix}_{ab} [-i\sigma_y]_{\alpha, \beta} \langle b, \mu, \beta | n, -k, -\vec{M}_\perp \rangle^*. \quad (24)$$

Here  $a, b$  are the sublattice index and  $\begin{bmatrix} 0 & 1 \\ 1 & 0 \end{bmatrix}$  represents the exchange of A and B sites. In eq.(24), the orbital index  $\mu$  is unaffected by the time-reversal operator since we take the basis for orbitals to be *real*<sup>20</sup>. As a result, the flux for  $\vec{B}(\vec{M}_\perp, k_y)$  obeys  $\vec{B}(M_{\perp,x}, M_{\perp,y}, k_y) = -\vec{B}(-M_{\perp,x}, -M_{\perp,y}, -k_y)$ , as is seen in Fig.6.

In the center of this figure,  $(M_{\perp,x}, M_{\perp,y}, k_y) = (0, 0, 0)$ , there is a source of the flux, i.e., a magnetic monopole. This is the band touching point between the HVB ( $n = 3$ ) and the LCB ( $n = 4$ ) as seen in the Fig.7(b). Since the collinear antiferromagnet ( $\vec{M}_\perp = 0$ ) is invariant under  $\{R|a_y\}$ , this band touching point is nothing but the Kramers doublet. Namely, when we take  $k$  and  $\vec{M}_\perp$  to

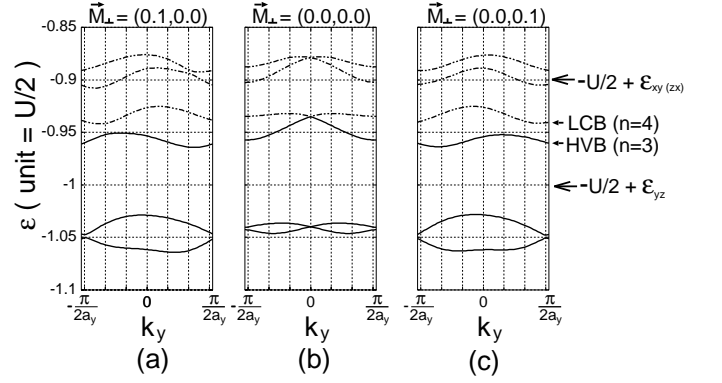


FIG. 7: Energy dispersions of the lower 6 bands, which are mainly composed of  $t_{2g}$  orbitals and constitute the lower Hubbard bands. Here we take the same parameter values as those in Fig.6. The broken lines denote those of the empty bands, while the solid lines represent the filled bands.

be zero, both the r.h.s. and l.h.s. in eq.(24) are the magnetic Bloch wavefunctions at  $k = \vec{M}_\perp = 0$  with the same eigenenergy and are orthogonal to each other. The applied magnetic field produces a finite magnetization  $\vec{M}_\perp$  and breaks this degeneracy as in Fig.7(a),(c). Therefore the existence of this monopole is independent of the details of our model and the consequence of the time-reversal symmetry, which is broken by the finite  $\vec{M}_\perp$ . When we take the surface integral of this flux over the sphere which encloses this monopole, we obtain  $+2\pi$ . Correspondingly, the adiabatic deformation along the path  $\Gamma_{cyc}$ , which encloses  $\vec{M}_\perp = 0$  clockwise as in Fig.6, results in the quantized change of the electronic polarization, i.e.,  $\Delta_{\Gamma_{cyc}} P_{y,el} = +e$ . However when we fill also the other band  $n = 4$ , i.e., 4 electrons per single MUC, the situation is different. Since this degeneracy point also becomes a sink of the flux  $\vec{B}_{n=4}$ , the direction of  $\vec{B}_{n=4}$  is opposite to that of  $\vec{B}_{n=3}$ . Because these fluxes are summed up for the electronic polarization,  $\vec{B}_{n=3}$  and  $\vec{B}_{n=4}$  cancel each other when we fill up to the  $n = 4$  band<sup>19</sup>.

Let us generalize the above 1D studies into the 2D case. We introduce the kinetic potential along the  $x$ -direction given by a following form,

$$H_{K,x\text{-direction}} = \Delta \sum_{\mu, \nu} C_{i_x + a_x, i_y, \mu, \alpha}^\dagger [t^{x,s}]_{\mu, \nu} C_{i_x, i_y, \nu, \alpha} + c.c. \quad (25)$$

$$\text{where } [t^{x,s}] = \begin{bmatrix} -t_0 & t_1 & 0 & 0 & 0 \\ t_1 & -t_2 & 0 & 0 & 0 \\ 0 & 0 & -t_5 & 0 & 0 \\ 0 & 0 & 0 & 0 & 0 \\ 0 & 0 & 0 & 0 & -t_5 \end{bmatrix}$$

where we ignore the antisymmetric transfer integrals coming from the oxygen shifts, because they do not change the conclusion essentially if they are not so strong.  $\Delta$  represents the anisotropy in transfer integral between  $x$ - and  $y$ -directions. Then the electronic polarization of  $y$ -

component  $\frac{\partial P_{y,\text{el}}}{\partial \vec{M}_\perp}$  in eq.(7) requires another integral with

respect to the crystal momentum  $k_x$ ,

$$\begin{aligned}
\frac{\partial P_{y,\text{el}}}{\partial \vec{M}_\perp} \cdot \delta \vec{M}_\perp &= \int_{-\frac{\pi}{2a_x}}^{\frac{\pi}{2a_x}} \frac{dk_x}{2\pi} \frac{\partial P_{y,\text{el}}(k_x)}{\partial \vec{M}_\perp} \cdot \delta \vec{M}_\perp \\
&= ie \frac{1}{(2\pi)^2} \int_{-\frac{\pi}{2a_x}}^{\frac{\pi}{2a_x}} dk_x \int_{-\frac{\pi}{2a_y}}^{\frac{\pi}{2a_y}} dk_y \sum_{n:\text{VB}} \left( \frac{\partial}{\partial k_y} \langle n, k_x, k_y, \vec{M}_\perp | \frac{\partial}{\partial \vec{M}_\perp} | n, k_x, k_y, \vec{M}_\perp \rangle - \text{c.c.} \right) \cdot \delta \vec{M}_\perp \\
&= \int_{-\frac{\pi}{2a_x}}^{\frac{\pi}{2a_x}} \frac{dk_x}{2\pi} \frac{e}{2\pi} \int_{\delta \vec{M}_\perp \times [-\frac{\pi}{2a_y}, \frac{\pi}{2a_y}]} d\vec{S} \cdot \sum_{n:\text{VB}} \vec{B}_n(k_x, k_y, M_{\perp,x}, M_{\perp,y}).
\end{aligned} \tag{26}$$

For example, the total change of the electronic polarization after the cyclic deformation of  $\vec{M}_\perp$ , i.e.,  $\oint_{\Gamma_{\text{cyc}}} dP_{y,\text{el}}$  will be an integer times  $\frac{e}{a_x}$  when  $\Delta_{\Gamma_{\text{cyc}}} P_{y,\text{el}}(k_x) \equiv \oint_{\Gamma_{\text{cyc}}} \frac{\partial P_{y,\text{el}}(k_x)}{\partial \vec{M}_\perp} \cdot d\vec{M}_\perp$  stays a constant (an integer times  $e$ ) for every  $k_x$ . Since there is a relation;  $H_{2D}(k_x = \pm \frac{\pi}{2a_x}, k_y, M_{\perp,x}, M_{\perp,y}) = H_{1D}(k_y, M_{\perp,x}, M_{\perp,y})$ , the distributions of the flux  $\vec{B}_n(k_x = \pm \frac{\pi}{2a_x}, k_y, M_{\perp,x}, M_{\perp,y})$  for each energy band are exactly same as those of the preceding 1D case. Namely, at  $(k_y, M_{\perp,x}, M_{\perp,y}) = (0, 0, 0)$ , there are always the monopole and/or antimonopole of the flux for each energy band as in Fig.6. When  $k_x$  is regarded as just an additional parameter, we can speculate that the deviation of  $k_x$  from  $k_x = \pm \frac{\pi}{2a_x}$  does not destroy these magnetic monopole and/or anti-monopole, since the doubly degenerate *point* in the  $k_y - M_{\perp,x} - M_{\perp,y}$  space forms a degeneracy *line* in a  $k_x - k_y - M_{\perp,x} - M_{\perp,y}$  space. Furthermore, the simple analysis given in the appendix C shows that this double degeneracy occurs on the line  $\vec{M}_\perp = k_y = 0$ . Thus for every  $k_x = \text{constant}$  plane, we always find a doubly degenerate point at  $\vec{M}_\perp = k_y = 0$  as in the preceding 1D studies. By using eq.(26), we obtain the  $y$ -component of the electronic polarization  $\frac{\partial P_{y,\text{el}}}{\partial \vec{M}_\perp}$  numerically as shown in Fig.8(a). In this calculation, we also fill 3 electrons per single MUC as in the preceding calculation in the 1D case.

At the center of this flow diagram, we find the vortex which results from the magnetic monopole found in Fig.6. The contour integral of this vector field around the arbitrary loop  $\Gamma_{\text{cyc}}$  enclosing this vortex clockwise produces  $+\frac{e}{a_x}$ . This is because  $\Delta_{\Gamma_{\text{cyc}}} P_{y,\text{el}}(k_x)$  is  $+e$  for every  $k_x$ , since we always find the source of the flux at  $\vec{M}_\perp = k_y = 0$ . However it is noted that near the center of this diagram ( $|\vec{M}_\perp| < 0.2$ ), the indirect gap closes and eq.(3) cannot be applied.

The magnitude of  $\frac{\partial P_{y,\text{el}}}{\partial \vec{M}_\perp}$  become larger when the direct energy gap become smaller than the other regions. For example, we show the behavior of  $\frac{\partial P_{y,\text{el}}(|\vec{M}_\perp|, \theta)}{\partial \theta}$  as a function of  $\theta$  for several constant  $|\vec{M}_\perp|$  in Fig.8(b), where  $\frac{\partial P_{y,\text{el}}(|\vec{M}_\perp|, \theta)}{\partial \theta}$  enhances at  $\theta = 0.5 \sim 0.6$  in case of

$|\vec{M}_\perp| = 0.2$  due to the reduction of the direct band gap. When we stack this 2D system in  $z$ -direction and constitute 3D layered system without an interlayer coupling, the order of  $\frac{\partial P_{y,\text{el}}(|\vec{M}_\perp|, \theta)}{\partial \theta}$  is around  $\frac{e}{a_x \cdot a_z} \sim 1[\text{C/m}^2]$  in case of  $a_x = a_z = 4\text{\AA}$ , which is much larger than the typical value  $\sim 10^{-5}[\text{C/m}^2]$  of the conventional Magneto-Electric materials as discussed in the introduction. When we fill odd number of electrons per single MUC, the flow of  $\frac{\partial P_{y,\text{el}}}{\partial \vec{M}_\perp}$  shows a similar behavior, in which there is always a vortex at  $\vec{M}_\perp = 0$  originating from the broken time-reversal symmetry. When  $\vec{\varphi}_{AF}$  is parallel to the  $z$ -axis, another degeneracy spoils the story which is explained in the Appendix D.

Finally, we want to mention about the relation between the dielectric property in our models and the conventional ME effect where broken  $IR$  by an applied magnetic field produces an electric polarization. Our model with the oxygen atoms shifted uniformly breaks both the spatial inversion symmetry  $I$  and its combination with the time-reversal symmetry  $IR$  over the whole phase diagram spanned by  $\vec{M}_\perp$ . Thus our observation is not included in the ME effect in a strict sense. However the electric polarization is allowed from the symmetry point of view over the entire region in Fig.8(a), and an applied magnetic field produces an interesting electric response where a cyclic deformation of the background spin configuration screws up electrons toward a particular direction. Thus we might call this phenomenon ME effect in a wider sense.

#### IV. CONCLUSION

In this article, we have studied the new mechanism for a gigantic Magneto-Electric (ME) effect. This is due to the geometrical Berry phase of the Bloch electrons, which is represented by the flux in the generalized momentum space including the external parameters such as the direction of the sublattice magnetization. Two models are proposed, one is the screw spins without spin orbit interaction (III-A) and the other is the multi-band models

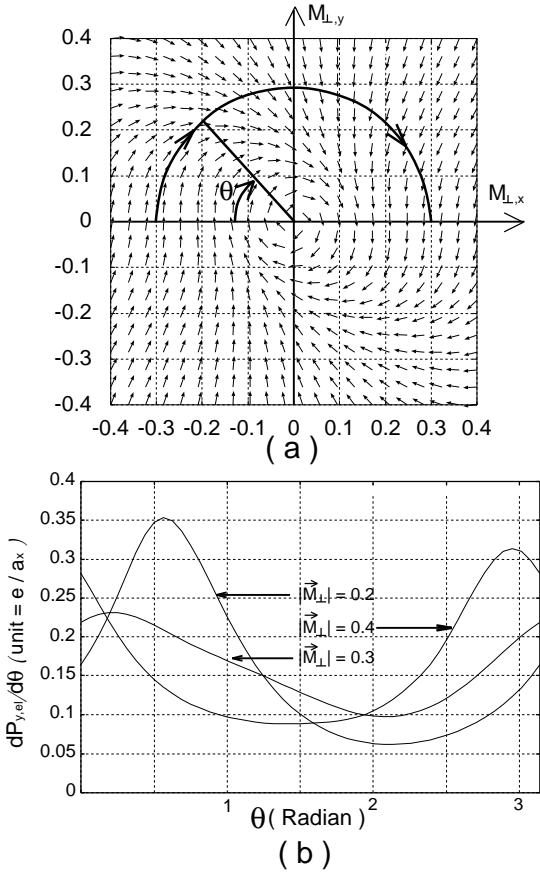


FIG. 8: (a) The flow of  $dP_y(\vec{M}_\perp)/d\vec{M}_\perp$  in the 2D case. Here we take  $\Delta = 0.2$ , while we take same parameter values as in Fig.6 as for the other parameters. Here the magnitudes of the vectors are normalized to be the same, while their magnitude can be reconstructed with the aid of (b). (b)  $dP_y(|\vec{M}_\perp| = \text{constant}, \theta)/d\theta$  as a function of  $\theta$ , where  $\theta$  is defined in (a).

The change of the electronic polarization  $\delta\vec{P}_{\text{el}}$  given in eq.(5) is naturally derived as a total charge transport vector  $\vec{Q}$ , as we will show in the following<sup>8</sup>. When the perturbation  $\delta H$  is introduced adiabatically from  $t = -\infty$  to  $t = t$ , the ground state wavefunction  $|\Psi(t)\rangle$  can be expanded by the eigenstate  $|\Psi_m\rangle$  at  $t = -\infty$ .

$$i\frac{\partial}{\partial t}|\Psi(t)\rangle = \left(\hat{H} + \frac{1}{2}\delta\hat{H}e^{i(\omega-i\delta)t} + \frac{1}{2}\delta\hat{H}e^{i(-\omega-i\delta)t}\right)|\Psi(t)\rangle$$

$$|\Psi(t)\rangle = |\Psi_0\rangle e^{-iE_0 t} + \sum_{m \neq 0} |\Psi_m\rangle a_m(t) e^{-iE_m t},$$

$$\text{where } a_m(t) = -\frac{1}{E_m - E_0 + \omega - i\delta} e^{i(E_m - E_0 + \omega - i\delta)t} \langle \Psi_m | \frac{1}{2} \delta \hat{H} | \Psi_0 \rangle$$

$$- \frac{1}{E_m - E_0 - \omega - i\delta} e^{i(E_m - E_0 - \omega - i\delta)t} \langle \Psi_m | \frac{1}{2} \delta \hat{H} | \Psi_0 \rangle.$$

Thus the electronic current density at time  $t$ ,  $\frac{1}{V} \langle \Psi(t) | \hat{J}_{\text{el}} | \Psi(t) \rangle$ , is given up to the first order in  $\delta \hat{H}$  as

$$\frac{1}{V} \langle \Psi(t) | \hat{J}_{\text{el}} | \Psi(t) \rangle = \frac{2}{V} \sum_{m \neq 0} \text{Re}[a_m(t) e^{-i(E_m - E_0)t} \langle \Psi_0 | \hat{J}_{\text{el}} | \Psi_m \rangle]$$

with the spin-orbit interaction (III-B). In both of these models, a magnetic monopole and an anti-monopole appear in this generalized momentum space, which determine the distribution of the flux. This (anti)monopole corresponds to the degeneracy of the two bands. In the first model (III-A) we found the species doubling, i.e., a magnetic monopole and an anti-monopole always appear in pairs in the compact 3D parameter space. In the second model (III-B), the monopole is attributed to the Kramers doublet, where the broken time-reversal symmetry in addition to the broken spatial inversion symmetry is essential. This means that the ME effect is not simply determined by the magnitude of the energy gap, and the geometrical structure of the U(1) gauge associated with the Bloch wavefunctions also plays an important role. A comparison with the conventional ME effect<sup>6</sup> suggests that the magnitude could be  $\sim 10^5$  times larger when the monopole's contribution to the electronic polarization survives. Although we do not have an explicit candidate, it would be very interesting to look for the material where this mechanism of gigantic ME effect works. The detailed band structure calculations will be helpful to reveal the distribution of the flux in the generalized momentum space, which are left for future studies.

#### Acknowledgments

The authors acknowledge S. Ishihara, Z.Fang, T.Egami S.Murakami, M.Onoda, and Y.Tokura for fruitful discussions. This work is supported by Grant-in-Aids from the Ministry of Education, Culture, Sports, Science, and Technology of Japan.

#### APPENDIX A: THE INTEGRATED ELECTRON CURRENT

$$\begin{aligned} &= \vec{j}_{el}(\omega)e^{i(\omega-i\delta)t} + \text{c.c.} \\ \vec{j}_{el}(\omega) &= -\frac{1}{V} \sum_{m \neq 0} \left( \frac{\langle \Psi_0 | \hat{J}_{el} | \Psi_m \rangle \langle \Psi_m | \frac{1}{2} \delta \hat{H} | \Psi_0 \rangle}{E_m - E_0 + \omega - i\delta} + \frac{\langle \Psi_m | \hat{J}_{el} | \Psi_0 \rangle \langle \Psi_0 | \frac{1}{2} \delta \hat{H} | \Psi_m \rangle}{E_m - E_0 - (\omega - i\delta)} \right). \end{aligned} \quad (\text{A1})$$

Here we omitted  $\langle \Psi_0 | \hat{J}_{el} | \Psi_0 \rangle$ , since the system is an insulator at  $t = -\infty$ . We define a total charge transport vector  $\vec{Q}$  as an integral of this electronic current density  $\frac{1}{V} \langle \Psi(t) | \hat{J}_{el} | \Psi(t) \rangle$  from  $t = -\infty$  to  $t = 0$ . The magnitude of  $\vec{Q}$  represents the total charges which pass through a unit area normal to  $\vec{Q}$  while  $\delta \hat{H}$  is introduced adiabatically. This vector  $\vec{Q}$  can be calculated as follows,

$$\begin{aligned} \vec{Q} &= \frac{1}{V} \int_{-\infty}^0 \langle \Psi(t) | \hat{J}_{el} | \Psi(t) \rangle dt \\ &= \frac{1}{i(\omega - i\delta)} (\vec{j}_{el}(\omega) - \vec{j}_{el}(\omega = 0)) + \text{c.c.} \end{aligned}$$

Here we subtracted  $2\pi\delta(\omega)\vec{j}_{el}(\omega = 0)$  from  $\vec{Q}$ , since we assume that the system remains an insulator from  $t = -\infty$  to  $t = 0$ . When we take the static limit ( $\omega \rightarrow 0$ ),  $\vec{Q}$  is shown to be equal to  $\delta \vec{P}_{el}$  in eq.(5)

## APPENDIX B: FICTITIOUS MAGNETIC CHARGE

In this appendix, I will show the relation between the doubly degenerate point given in eq.(12) and the fictitious magnetic charge associated with the flux defined in eqs.(8,9). In the region where the  $n$ -th band does not form degeneracy between its neighboring bands, there is no magnetic charge, i.e.,  $\vec{\nabla} \cdot \vec{B}_n = \vec{\nabla} \cdot \vec{\nabla} \times \vec{A}_n = 0$ . Thus the surface-integral of the flux over the sphere within which the flux is well-defined becomes zero by the Gauss law. However, the flux in eqs.(8,9) is not defined in the region where the  $n$ -th band forms degeneracy between its neighboring band as in eq.(12). In the followings, we will show that the surface-integral of the flux over an infinitesimally sphere enclosing this doubly degenerate point becomes quantized to be  $\pm 2\pi$ . When the  $3 \times 3$  matrix  $V$  in eq.(12) is orthogonal, an appropriate SU(2) rotation, i.e.,  $e^{i\theta \vec{n} \cdot [\vec{\sigma}]} \cdot [H]_{2 \times 2} \cdot e^{-i\theta \vec{n} \cdot [\vec{\sigma}]}$  make this  $3 \times 3$  matrix  $V$  diagonal, i.e., that given in eq.(B2). Since we assume  $V$  is independent of  $\vec{K}$  and so is this rotation, the flux defined in eqs.(8,9) is invariant under this SU(2) rotation. Thus the flux is given by eq.(B5) with  $\vec{K}'$  replaced by  $\vec{K}$ . After the surface-integral over the sphere enclosing this doubly degenerate point, i.e.,  $\vec{K} = 0$ , we obtain eq.(B6). Even when the matrix  $V$  is not orthogonal, the situation will reduce to a similar one as in case of othogonal by the following procedure. First, we consider the surface-integral of the flux over an infinitesimally small box  $v = \{(K_x, K_y, K_z) | (K_x, K_y, K_z) \in$

$[-\delta_x, \delta_x] \times [-\delta_y, \delta_y] \times [-\delta_z, \delta_z]\}$  enclosing this degenerate point, i.e.,

$$\int \int_{\partial v} d\vec{S} \cdot \vec{B}_n(\vec{K}). \quad (\text{B1})$$

Here we take the vector  $d\vec{S}$  to be directed from inside to outside of the box. When we define a new coordinate,

$$\begin{aligned} \begin{bmatrix} K'_x \\ K'_y \\ K'_z \end{bmatrix} &= \begin{bmatrix} 1 & & \\ & \text{sign}(\det V) & \\ & & 1 \end{bmatrix} \cdot [V] \cdot \begin{bmatrix} K_x \\ K_y \\ K_z \end{bmatrix} \\ &\equiv [T] \cdot \begin{bmatrix} K_x \\ K_y \\ K_z \end{bmatrix} \end{aligned}$$

the  $2 \times 2$  effective Hamiltonian given in eq.(12) can be given as follows,

$$[H]_{2 \times 2} = K'_x[\sigma_x] + \text{sign}(\det V) \cdot K'_y[\sigma_y] + K'_z[\sigma_z], (\text{B2})$$

where we omitted the term which is propotional to unit matrix. Then the flux in this new coordinate,  $\vec{B}'_n(\vec{K}')$ , and the its relation between the flux  $\vec{B}_n(\vec{K})$  are given as follows.

$$\begin{aligned} \vec{B}'_n(\vec{K}') &= -i \nabla_{\vec{K}'} \times \langle n, \vec{K}' | \vec{\nabla}_{\vec{K}'} | n, \vec{K}' \rangle \\ B_{n,\mu}(\vec{K}) &= \det T \sum_{\nu} [T^{-1}]_{\mu,\nu} B'_{n,\nu}(\vec{K}') \\ &= \sum_{\nu} \tilde{a}_{\nu,\mu} B'_{n,\nu}(\vec{K}'), \end{aligned}$$

where  $\tilde{a}_{\nu,\mu}$  is the  $(\nu,\mu)$ -th cofactor of the  $3 \times 3$  matrix  $[T]$ . The integral in eq.(B1) consists of the surface-integral over the 6 rectangulars. For example, the integral of the flux over the rectangular  $X_+ \equiv \{(K_x, K_y, K_z) | K_x = \delta_x, (K_y, K_z) \in [-\delta_y, \delta_y] \times [-\delta_z, \delta_z]\}$  can be transformed as follows;

$$\begin{aligned} &\int \int_{X_+} dK_y dK_z B_{n,x} \\ &= \int \int_{T(X_+)} d\vec{S}' \cdot \vec{B}'_n(\vec{K}'). \end{aligned} \quad (\text{B3})$$

Here the direction of  $d\vec{S}'$  was also taken so that it penetrates the parallelogram  $T(X_+)$  from inside to outside of the box  $T(v)$ . In order to derive eq.(B3), we used the following identities;

$$dK_y dK_z B_{n,x}$$

$$\begin{aligned}
&= dK_y dK_z (\tilde{a}_{xx} B'_{n,x} + \tilde{a}_{yx} B'_{n,y} + \tilde{a}_{zx} B'_{n,z}) \\
&= \begin{pmatrix} T_{xy} \\ T_{yy} \\ T_{zy} \end{pmatrix} dK_y \times \begin{pmatrix} T_{xz} \\ T_{yz} \\ T_{zz} \end{pmatrix} dK_z \cdot \begin{bmatrix} B'_{n,x} \\ B'_{n,y} \\ B'_{n,z} \end{bmatrix} \\
&= d\vec{S}' \cdot \vec{B}'_n,
\end{aligned} \tag{B5}$$

where we bear in mind that the parallelogram  $T(X_+)$  is subtended by  $\begin{bmatrix} T_{xy} \\ T_{yy} \\ T_{zy} \end{bmatrix} dK_y$  and  $\begin{bmatrix} T_{xz} \\ T_{yz} \\ T_{zz} \end{bmatrix} dK_z$  and that the  $3 \times 3$  matrix  $[T]$  is positive definite by definition. The other surface-integrals over remaining 5 faces can be also transformed in a similar way and as results eq.(B1) can be rewritten as follows.

$$\begin{aligned}
\text{eq.(B1)} &= \int \int_{\partial T(v)} d\vec{S}' \cdot \vec{B}'_n(\vec{K}') \\
&= \int \int_S d\vec{S}' \cdot \vec{B}'_n(\vec{K}'), \tag{B4}
\end{aligned}$$

where  $S$  is the sphere enclosing the origin,  $\vec{K}' = 0$ . Since  $\vec{B}'_n(\vec{K}')$  is the flux associated with the eigenvector of eq.(B2), the r.h.s. of eq.(B4) can be calculated easily. By using the spherical coordinate;  $(K'_x, K'_y, K'_z) = K'(\sin \theta \cos \phi, \sin \theta \sin \phi, \cos \theta)$ , the eigenvector of eq.(B4) can be given as follows,

$$|n, \vec{K}'\rangle = \begin{cases} \begin{bmatrix} \cos \frac{\theta}{2} \\ \sin \frac{\theta}{2} e^{i\phi \cdot \text{sign}(\det V)} \\ \sin \frac{\theta}{2} e^{-i\phi \cdot \text{sign}(\det V)} \end{bmatrix}, & \text{for } E_n = K' \\ \begin{bmatrix} \cos \frac{\theta}{2} \\ \sin \frac{\theta}{2} e^{-i\phi \cdot \text{sign}(\det V)} \\ -\cos \frac{\theta}{2} \end{bmatrix}. & \text{for } E_n = -K' \end{cases}$$

Since the eigenvectors are independent of  $K'$ , the flux can be calculated easily,

$$\vec{B}'_n(\vec{K}') = \frac{1}{K'^2 \sin \theta} \left( \frac{\partial}{\partial \theta} \langle n, \vec{K}' | \frac{\partial}{\partial \phi} | n, \vec{K}' \rangle - \text{c.c.} \right) \frac{\vec{K}'}{K'}$$

where the sign + is for the case when the  $n$ -th band is the upper band and the sign - is for the lower band. Substituting the result in eq.(B5) into the r.h.s. of eq.(B4), we get

$$\begin{aligned}
&\int \int_{\partial v} d\vec{S} \cdot \vec{B}_n(\vec{K}) \\
&= \pm 2\pi \cdot \text{sign}(\det V), \tag{B6}
\end{aligned}$$

where  $\pm$  correspond to those in eq.(B5) respectively. To be summarized, in case of  $\det V < 0$ , the flux for the upper band sinks into the point,  $\vec{K} = 0$ , while that for the lower band streams from this origin with  $2\pi$  charge. But in case of  $\det V > 0$ , the above relations are reversed.

### APPENDIX C: $\vec{\varphi}_{AF}$ COLLINEAR TO AN ARBITRARY DIRECTION

The identification of the doubly degenerate region in the parameter space is very important to understand the distribution of the flux and/or to construct the model which exhibits non-trivial topological structures of the flux. In the following two appendices, we will explain how to identify the doubly degenerate point or line in the generalized momentum space defined in the section III-B. In this Appendix, we will show that a double degeneracy always occurs on the line;  $\vec{M}_\perp = k_y = 0$  in the  $k_x - k_y - \vec{M}_\perp$  space. The Hamiltonian in the 2D case given in the section III-B is rewritten in the momentum representation as follows;

$$\begin{aligned}
H &= \sum [H(\vec{k}, \vec{\varphi}_{AF}, \vec{M}_\perp)]_{(a,\mu,\alpha|b,\nu,\beta)} f_{\vec{k},a,\mu,\alpha}^\dagger f_{\vec{k},b,\nu,\beta} \\
&\text{where } [H(\vec{k}, \vec{\varphi}_{AF}, \vec{M}_\perp)]_{(a,\mu,\alpha|b,\nu,\beta)} = \epsilon_\mu \delta_{a,b} \delta_{\mu,\nu} \delta_{\alpha,\beta} + 2 \cos(k_y a_y) \begin{bmatrix} 0 & 1 \\ 1 & 0 \end{bmatrix}_{a,b} [\mathbf{t}^{y,s}]_{\mu,\nu} \delta_{\alpha,\beta} \\
&+ 2 \Delta \cos(k_x a_x) \begin{bmatrix} 0 & 1 \\ 1 & 0 \end{bmatrix}_{a,b} [\mathbf{t}^{x,s}]_{\mu,\nu} \delta_{\alpha,\beta} + 2 \sin(k_y a_y) \begin{bmatrix} 0 & -i \\ i & 0 \end{bmatrix}_{a,b} [\mathbf{t}^{y,a}]_{\mu,\nu} \delta_{\alpha,\beta} \\
&+ \sum_{\lambda=x,y,z} \begin{bmatrix} 1 & 0 \\ 0 & 1 \end{bmatrix}_{a,b} [\mathbf{L}\lambda]_{\mu,\nu} [\boldsymbol{\sigma}\lambda]_{\alpha,\beta} + \sum_{\lambda=x,y,z} \begin{bmatrix} (\vec{\varphi}_{AF} + \vec{M}_\perp)_\lambda & 0 \\ 0 & (-\vec{\varphi}_{AF} + \vec{M}_\perp)_\lambda \end{bmatrix}_{a,b} \delta_{\mu,\nu} [\boldsymbol{\sigma}\lambda]_{\alpha,\beta}. \tag{C1}
\end{aligned}$$

Here  $a, b$  are the sublattice,  $\mu, \nu$  are the orbital, and  $\alpha, \beta$  are the spin indices, respectively. Here the  $5 \times 5$  matrix  $[\mathbf{t}^{y,s}]$ ,  $[\mathbf{t}^{y,a}]$  and  $[\mathbf{t}^{x,s}]$  are explicitly given in eqs.(21),(25). When we take  $\vec{M}_\perp = 0$ , our Hamiltonian is invariant under the time-reversal symmetry  $R$  accompanied by spatial translation  $T_{\vec{a}_y}$ , i.e.,  $\{R|a_y\}$  as is seen in Fig.5(a). This

means that  $H(k_x, k_y, \vec{\varphi}_{AF}, \vec{M}_\perp = 0)$  obeys the following equation,

$$\begin{aligned} \sum_{a', \alpha'} \sum_{b', \beta'} \begin{bmatrix} 0 & 1 \\ 1 & 0 \end{bmatrix}_{a, a'} [-i\sigma_{\mathbf{y}}]_{\alpha, \alpha'} \cdot [H(k_x, k_y, \vec{\varphi}_{AF}, \vec{M}_\perp = 0)]_{(a', \mu, \alpha' | b', \nu, \beta')} \cdot [i\sigma_{\mathbf{y}}]_{\beta', \beta} \begin{bmatrix} 0 & 1 \\ 1 & 0 \end{bmatrix}_{b', b} \\ = [H(-k_x, -k_y, \vec{\varphi}_{AF}, \vec{M}_\perp = 0)]_{(a, \mu, \alpha | b, \nu, \beta)}^* \end{aligned}$$

where  $\begin{bmatrix} 0 & 1 \\ 1 & 0 \end{bmatrix}$  corresponds to the spatial translation  $T_{a_y}$  and represents the exchange of A and B sublattices.

Since we neglect the antisymmetric transfer integrals along the  $x$ -direction, we can change the sign of  $k_x$  in eq.(C1), i.e.,  $[H(-k_x, -k_y)] = [H(k_x, -k_y)]$ . As a result, both  $\langle a, \mu, \alpha | n, k_x, k_y = 0, \vec{\varphi}_{AF}, \vec{M}_\perp = 0 \rangle$  and  $\sum_{b, \beta} \begin{bmatrix} 0 & 1 \\ 1 & 0 \end{bmatrix}_{a, b} [-i\sigma_{\mathbf{y}}]_{\alpha, \beta} \langle \mu, \beta | n, k_x, k_y = 0, \vec{\varphi}_{AF}, \vec{M}_\perp = 0 \rangle^*$  become the eigenstate of  $[H(k_x, k_y = 0, \vec{\varphi}_{AF}, \vec{M}_\perp = 0)]$  with the same energy and they are orthogonal to each other. Thus, a double degeneracy is assured on the line  $\vec{M}_\perp = k_y = 0$ .

#### APPENDIX D: $\vec{\varphi}_{AF}$ COLLINEAR TO THE $z$ -DIRECTION

In this Appendix, we will show that another double degeneracy occurs at  $(k_x, k_y) = (\frac{\pi}{2a_x}, \pm \frac{\pi}{2a_y}) \equiv \vec{k}_X$  in the 4D space spanned by  $k_x, k_y, \vec{M}_\perp$ , when the AF moment  $\vec{\varphi}_{AF}$  is collinear to the  $z$ -direction. When  $\vec{M}_\perp = 0$  with the  $\vec{\varphi}_{AF}$  collinear to the  $z$ -direction, the system is invariant under  $\{E, \{\sigma_y | a_y\}, IC_{2z}, \{C_{2x} | a_y\}\}$  in addition to  $\{R | a_y\}$ . Here  $I, \sigma_\mu$  and  $C_{2\nu}$  represent the spatial inversion, the mirror with respect to the  $\mu = 0$  plane and the spatial rotation by  $\pi$  around the  $\nu$ -axis respectively. The  $k$ -group at  $\vec{k}_X$  is composed of an unitary subgroup  $G_{\vec{k}_X} \equiv T_{\vec{R}_l} \times \{E, IC_{2z}\}$  and an antiunitary subgroup  $\{R | a_y\} \times T_{\vec{R}_l} \times \{E, IC_{2z}\}$ . The irreducible representation of an unitary subgroup  $T_{\vec{R}_l} \times \{E, IC_{2z}\}$  is  $e^{i\vec{k}_X \cdot \vec{R}_l} \Gamma_{C_{1h}}(\{E, IC_{2z}\})$ , where  $\Gamma_{C_{1h}}$  means the representation of the monoclinic point group  $C_{1h}$  and its character table is given by

$C_{1h}$	$E$	$\bar{E}$	$IC_{2z}$	$I\bar{C}_{2z}$
$\Gamma_3$	1	-1	-i	i
$\Gamma_4$	1	-1	i	-i

Here we only take the double-valued representation since we treat the spinful Hamiltonian with the spin-orbit interaction.  $\bar{E}$  represents the  $2\pi$  rotation in the  $\frac{1}{2}$ -spin space and  $I\bar{C}_{2z} = \bar{E}IC_{2z}$ . The dimensionality of these two representations are doubled by the presence of the antiunitary subgroup,  $\{R | a_y\} \times T_{\vec{R}_l} \times \{E, IC_{2z}\}$ , according to the Wigner's criterion<sup>21</sup>, i.e.,

$$\begin{aligned} \sum_{u \in G_{\vec{k}_X}, \bar{E}G_{\vec{k}_X}} \chi^{\vec{k}_X} ((\{R | a_y\} \cdot u)^2) \\ = 2 \sum_{\vec{R}_l} e^{2i\vec{k}_X \cdot (\vec{a}_y + \vec{R}_l)} (\Gamma_{3(4)}(R^2) + \Gamma_{3(4)}(R^2 C_{2z}^2)) \\ = 2 \sum_{\vec{R}_l} e^{2i\vec{k}_X \cdot (\vec{a}_y + \vec{R}_l)} (\Gamma_{3(4)}(\bar{E}) + \Gamma_{3(4)}(E)) = 0. \end{aligned}$$

Thus only 2-dimensional representations are allowed at  $\vec{k}_X$ . These degeneracies still remain even when we violate the time-reversal symmetry  $\{R | a_y\}$  by introducing a finite  $\vec{M}_\perp$ . In case of the finite  $\vec{M}_\perp$ , the system is still invariant under the  $T_{\vec{R}_l} \times \{E, \{RIC_{2z} | a_y\}\}$ , since both  $IC_{2z}$  and  $\{RIC_{2z} | a_y\}$  change the sign of  $\vec{M}_\perp$  as seen in Fig.5(a),(b). In the same way as in case of  $\vec{M}_\perp = 0$ , the degeneracy at  $\vec{k}_X$  are doubled by the antiunitary k-group at  $\vec{k}_X$ , because

$$\begin{aligned} \sum_{u = T_{\vec{R}_l} \times \{E, \bar{E}\}} \chi^{\vec{k}_X} ((\{RIC_{2z} | a_y\} \cdot u)^2) \\ = 2 \sum_{\vec{R}_l} e^{2i\vec{k}_X \cdot (\vec{R}_l + \vec{a}_y)} = -2N, \end{aligned}$$

where  $2N$  is the total number of the elements of the unitary k-group  $T_{\vec{R}_l} \times \{E, \bar{E}\}$ .

<sup>1</sup> I.E.Dzyaloshinskii, Sov. Phys. JETP. **10**, 628 (1960)

<sup>2</sup> G.T.Rado and V.J. Folen, Phys.Rev.lett. **7**, 310, (1961), J.appl.Phys. **33**, 1126S (1962)

<sup>3</sup> S.Alexander and S.Shtrikman, Solid State Comm. **4**, 115 (1965), R.Hornreich and S.Shtrikman, Phys. Rev. **161**, 506 (1967)

<sup>4</sup> M.Date, J.Kanamori and M.Tachiki J.Phys.Soc.Japan **16**, 2569 (1961)

<sup>5</sup> H.Yatom and R.Englman Phys.Rev. **188**,793 (1969)

<sup>6</sup> G.T.Rado, J.M.Ferrari, Phys.Rev.B **12**, 5166 (1975)

<sup>7</sup> R. D. King-Smith and D. Vanderbilt Phys. Rev. B. **47**, 1651 (1993).

<sup>8</sup> R. Resta, EuroPhys. Lett. **22** 133 (1993), Rev. Mod. Phys. **55**, 899 (1994)

<sup>9</sup> F. Bernardini, V. Fiorentini, and D. Vanderbilt, Phys. Rev. B **56**, R10024 (1997), L. Bellaiche and D. Vanderbilt, Phys.

Rev. Lett. **83**, 1347 (1999).

- <sup>10</sup> J.E.Avron et al, Phys. Rev. Lett. **78**, 511 (1997).  
<sup>11</sup> D.J.Thouless, Phys.Rev.B **27**, 6083 (1983), Q.Niu, D.J.Thouless, J.Phys.A **17**, 2453 (1984).  
<sup>12</sup> B.L.Altshuler, L.I.Galzman, Science **283**, 1864 (1999)  
<sup>13</sup> M.V.Berry, Proc.Roy.Soc.Lond.**A392**, 45 (1984)  
<sup>14</sup> M.Nakahara, *Geometry, topology and physics* (Institute of Physics Publishing, 1990)  
<sup>15</sup> K.Ohgushi, S.Murakami and N.Nagaosa, Phys. Rev. B **62**(10), R6065 (2000), Y.Taguchi, Y.Ohara, H.Yoshizawa, N.Nagaosa and Y.Tokura, Science **291**, 2573 (2001), R.Shindou and N.Nagaosa, Phys. Rev. Lett. **87** 116801 (2001), M.Onoda and N.Nagaosa, J. Phys. Soc. Jpn. **71**(1) 19 (2002)  
<sup>16</sup> D.J.Thouless, M.Kohmoto, M.P.Nightingale and M.den Nijs, Phys.Rev.Lett. **49**, 405 (1982), M.Kohmoto, Ann.Phys.(N.Y.) **160**, 343 (1985)  
<sup>17</sup> L.B.Nielsen and M.Ninomiya, Nucl.Phys. B **185**,20 (1981), **193**,173,(1981)  
<sup>18</sup> Before the antimonopole goes outside the cylinder, path  $\Gamma_{\text{cyc}}$  meets the metallic region where the band gap collapses and eqs.(3,5) become invalid.  
<sup>19</sup> Although  $\vec{B}_1$  and  $\vec{B}_2$  also contribute to the MEP, both of them are cancelled each other by the same reason as the cancellation between  $\vec{B}_3$  and  $\vec{B}_4$ .  
<sup>20</sup> The symmetry operators act on our Hamiltonian,  $\hat{H} = H_{(i,\mu,\alpha|j,\nu,\beta)} f_{i,\mu,\alpha}^\dagger f_{j,\nu,\beta}$ , as follows;

$$\begin{aligned}
 H_{(i,\mu,\alpha|j,\nu,\beta)} &\rightarrow \sum_{\mu',\mu'} \sum_{\alpha',\beta'} [R^{(t)}]_{\mu,\mu'}^{-1} [\sigma_y]_{\alpha,\alpha'} \\
 &\quad H_{(i,\mu',\alpha'|j,\nu',\beta')}^* [R^{(t)}]_{\nu',\nu} [-i\sigma_y]_{\beta',\beta} \\
 &\quad \text{(time - reversal operator } R \text{)} \\
 H_{(i,\mu,\alpha|j,\nu,\beta)} &\rightarrow \sum_{\mu',\mu'} \sum_{\alpha',\beta'} [e^{-i\theta\vec{n}\cdot\vec{L}}]_{\mu,\mu'} [e^{-i\theta\vec{n}\cdot\vec{S}}]_{\alpha,\alpha'} \\
 &\quad H_{(C(\vec{n},\theta)^{-1}(i),\mu',\alpha'|C(\vec{n},\theta)^{-1}(j),\nu',\beta')}
 \end{aligned}$$

$$\begin{aligned}
 &[e^{i\theta\vec{n}\cdot\vec{L}}]_{\nu',\nu} [e^{i\theta\vec{n}\cdot\vec{S}}]_{\beta',\beta} \\
 &\quad \text{( spatial rotation around } \vec{n} \text{ by } \theta : C(\vec{n},\theta) \text{ )}
 \end{aligned}$$

Here the indice  $i, j$  are the site indice (not only magnetic unit cell indice but also sublattice indice are included),  $\mu, \nu$  are those for orbitals and  $\alpha, \beta$  are those for spins. Here as for the operators on the orbital space, when the basis functions for d-orbital indice  $\mu$  and  $\nu$  are taken as  $|L^2 = 2(2+1), L_z = 2\rangle, |6, 1\rangle, |6, 0\rangle (\equiv |6, 0^*\rangle), |6, -1\rangle (\equiv |6, 1^*\rangle), |6, -2\rangle (\equiv |6, 2^*\rangle)$ , we take  $[R^{(t)}]$  in the time-reversal operators as

$$\begin{bmatrix} 0 & 0 & 0 & 0 & 1 \\ 0 & 0 & 0 & 1 & 0 \\ 0 & 0 & 1 & 0 & 0 \\ 0 & 1 & 0 & 0 & 0 \\ 1 & 0 & 0 & 0 & 0 \end{bmatrix}.$$

In the convention of this paper, we take the basis functions for d-orbital as real functions and then  $[R^{(t)}]$  must be identity. Correspondingly,  $5 \times 5$  matrices  $[\vec{L}]$  in the spatial rotational operators should be taken as in eq.(22). As for the operators on the spin space, we take  $\vec{S} = \frac{1}{2}\vec{\sigma}$ .  $C(\vec{n}, \theta)^{-1}(i)$  represents the site which transports onto the site  $i$  when we apply the spatial rotation by  $\theta$  around the axis,  $\vec{n}$ . In contrast to the above operations, the spatial inversion  $I$  affects only on the site index  $i$  because the  $d$ -orbitals are always even under  $I$ ,

$$H_{i,j} \rightarrow H_{I(i),I(j)} \quad \text{( Spatial Inversion } I \text{ )}$$

- <sup>21</sup> T.Inui,Y.Tanabe,Y.Onodera, *Group Theory and Its Applications in Physics*, Solid State Sciences 78, chapter.13.